


Formation of the Mouse Internal Capsule and Cerebral Peduncle: A Pioneering Role for Striatonigral Axons as Revealed in *Isl1* Conditional Mutants

Jacqueline M. Ehrman,^{1,5} Paloma Merchan-Sala,¹ Lisa A. Ehrman,^{1,2} Bin Chen,⁷ Hee-Woong Lim,^{3,6} Ronald R. Waclaw,^{1,2,6} and  Kenneth Campbell^{1,4,6}

¹Division of Developmental Biology, Cincinnati Children's Hospital Medical Center, Cincinnati, Ohio 45229, ²Experimental Hematology and Cancer Biology, Cincinnati Children's Hospital Medical Center, Cincinnati, Ohio 45229, ³Biomedical Informatics, Cincinnati Children's Hospital Medical Center, Cincinnati, Ohio 45229, ⁴Department of Neurosurgery, Cincinnati Children's Hospital Medical Center, Cincinnati, Ohio 45229, ⁵Medical Scientist Training Program, University of Cincinnati College of Medicine, Cincinnati, Ohio 45267, ⁶Department of Pediatrics, University of Cincinnati College of Medicine, Cincinnati, Ohio 45267, and ⁷Department of Molecular, Cell and Developmental Biology, University of California, Santa Cruz, Santa Cruz, California 95064

The projection neurons of the striatum, the principal nucleus of the basal ganglia, belong to one of the following two major pathways: the striatopallidal (indirect) pathway or the striatonigral (direct) pathway. Striatonigral axons project long distances and encounter ascending tracts (thalamocortical) while coursing alongside descending tracts (corticofugal) as they extend through the internal capsule and cerebral peduncle. These observations suggest that striatal circuitry may help to guide their trajectories. To investigate the developmental contributions of striatonigral axons to internal capsule formation, we have made use of *Sox8-EGFP* (striatal direct pathway) and *Fezf2-TdTomato* (corticofugal pathway) BAC transgenic reporter mice in combination with immunohistochemical markers to trace these axonal pathways throughout development. We show that striatonigral axons pioneer the internal capsule and cerebral peduncle and are temporally and spatially well positioned to provide guidance for corticofugal and thalamocortical axons. Using *Isl1* conditional knock-out (cKO) mice, which exhibit disrupted striatonigral axon outgrowth, we observe both corticofugal and thalamocortical axon defects with either ventral forebrain- or telencephalon-specific *Isl1* inactivation, despite *Isl1* not being expressed in either cortical or thalamic projection neurons. Striatonigral axon defects can thus disrupt internal capsule formation. Our genome-wide transcriptomic analysis in *Isl1* cKOs reveals changes in gene expression relevant to cell adhesion, growth cone dynamics, and extracellular matrix composition, suggesting potential mechanisms by which the striatonigral pathway exerts this guidance role. Together, our data support a novel pioneering role for the striatal direct pathway in the correct assembly of the ascending and descending axon tracts within the internal capsule and cerebral peduncle.

Key words: axon guidance; axon outgrowth; cerebral cortex; development; striatum; thalamus

Significance Statement

The basal ganglia are a group of subcortical nuclei with established roles in the coordination of voluntary motor programs, aspects of cognition, and the selection of appropriate social behaviors. Hence, disruptions in basal ganglia connectivity have been implicated in the motor, cognitive, and social dysfunction characterizing common neurodevelopmental disorders such as attention-deficit/hyperactivity disorder, autism spectrum disorder, obsessive-compulsive disorder, and tic disorder. Here, we identified a novel role for the striatonigral (direct) pathway in pioneering the internal capsule and cerebral peduncle, and in guiding axons extending to and from the cortex. Our findings suggest that the abnormal development of basal ganglia circuits can drive secondary internal capsule defects and thereby may contribute to the pathology of these disorders.

Received Nov. 18, 2021; revised Feb. 9, 2022; accepted Feb. 13, 2022.

Author contributions: J.M.E., P.M.-S., L.A.E., B.C., R.R.W., and K.C. designed research; J.M.E., P.M.-S., and K.C. performed research; J.M.E., P.M.-S., H.-W.L., and K.C. analyzed data; J.M.E. and K.C. wrote the paper.

This work was supported by the National Institutes of Health (NIH) Grant R01-MH-090740 to R.R.W. and K.C., J.M.E. is supported by NIH Grant F30-MH-123056. The Bin Chen laboratory is supported by NIH Grants R01-NS-089777 and R01-MH-094859. We thank Dr. X. Mu and the late Dr. W.H. Klein for providing the *Isl1^{flx/flx}* mice. We also thank Drs. Masato Nakafuku and Brian Gebelein for critical comments on the manuscript.

The authors declare no competing financial interests.

Correspondence should be addressed to Kenneth Campbell at kenneth.campbell@cchmc.org.

<https://doi.org/10.1523/JNEUROSCI.2291-21.2022>

Copyright © 2022 the authors

Introduction

The striatum serves as the principal input nucleus of the basal ganglia, a group of subcortical nuclei best known for their role in coordinating voluntary motor programs (Obeso et al., 2002). Receiving inputs from motor, sensory, and limbic regions, the basal ganglia also contribute to the selection of appropriate social behaviors and executive function (Pennartz et al., 2011; Báez-Mendoza and Schultz, 2013; Macpherson et al., 2014).

Malformations in striatal circuitry are thus implicated in the motor, social, and cognitive abnormalities present in common neurodevelopmental disorders such as autism spectrum disorder (ASD), attention-deficit/hyperactivity disorder, and obsessive-compulsive disorder (Langen et al., 2009; Leisman et al., 2014; Norman et al., 2016). Much of our knowledge of basal ganglia function comes from studying them in the context of neurodegeneration (e.g., Huntington's and Parkinson's diseases); however, our understanding of the developmental mechanisms underlying the initial establishment of basal ganglia circuitry is comparatively incomplete.

Striatal projection neurons (SPNs) are classified into two distinct output pathways that work in concert to mediate basal ganglia function. These two pathways are defined by their molecular profiles and connectivity (Gerfen and Surmeier, 2011). Dopamine receptor D₁ (DRD1) expressing striatonigral or direct pathway SPNs (dSPNs) extend their long-distance axons through the diencephalon to the substantia nigra pars reticulata (SNr) via the internal capsule. In contrast, DRD2 expressing striatopallidal or indirect pathway SPN (iSPN) axons project shorter distances, taking a polysynaptic route through the globus pallidus (GP) and subthalamic nucleus (STN) before reaching the SNr. Activity within both pathways ultimately converges on the cerebral cortex via the thalamus.

The path taken by striatal projections through the ventral forebrain, diencephalon, and midbrain is also populated by other major axonal tracts, including the reciprocal ascending and descending connections that comprise the internal capsule. This major white matter tract relays motor and sensory information to and from the cortex and consists of descending corticofugal axons (CFAs), which project from deep cortical layers to subcortical locations, and ascending thalamocortical axons (TCAs), which extend from the thalamus to cortical layer IV (De Carlos and O'Leary, 1992; Auladell et al., 2000). Descending CFAs can be further subdivided into corticothalamic axons (CTAs), projecting from layer VI to the thalamus, and corticosubcerebral axons, projecting from layer V to targets in the hindbrain and spinal cord (Molyneaux et al., 2007).

As CFAs and TCAs both course alongside striatal projections for portions of their trajectories, these populations may be involved in guiding each other. Supporting this notion, several mouse mutants with striatal defects also exhibit CTA or TCA abnormalities, such as *Ascl1*, *Dlx1/2*, *Ebf1*, and *Gsx1/2* mutants (Tuttle et al., 1999; Garel et al., 2002; Yun et al., 2003). Despite this growing evidence, subpallial contributions to internal capsule pathfinding are largely attributed to guidepost populations located within the ventral forebrain (López-Bendito et al., 2006; Bielle et al., 2011b; Lokmane et al., 2013). Definitive contributions from striatal projections, particularly those from dSPN axons traveling caudal to traditionally studied guidepost populations located within the medial ganglionic eminence (MGE), are less clear.

Given these data, we hypothesized that striatonigral axons help to guide CFAs and TCAs through the forming internal capsule and cerebral peduncle. To test this hypothesis, we here use BAC transgenic reporter murine lines to trace dSPN axons, CFAs, and TCAs throughout development and to define the normal spatiotemporal relationships between them. We additionally use a previously established mouse model of impaired striatonigral outgrowth (*Isl1* conditional knock-out (cKO) mice; Ehrman et al., 2013; Lu et al., 2014; Merchan-Sala et al., 2017) and find that they also exhibit broad internal capsule axon defects. In contrast, we show that disrupted CFA outgrowth, as seen in *Fezf2*

mutants (Chen et al., 2005; Molyneaux et al., 2005; Chen et al., 2008), does not result in direct pathway defects. Finally, we identify potential molecular candidates regulating dSPN-mediated guidance of CFAs and TCAs in *Isl1* cKOs. Together, our work implicates pioneer dSPN axons in the establishment of internal capsule/cerebral peduncle trajectories.

Materials and Methods

Animals

All animal care and protocols were conducted in accordance with guidelines provided by the Cincinnati Children's Hospital Medical Center Institutional Animal Care and Use Committee and the National Institutes of Health. Once obtained, mouse lines were crossed to and maintained on an outbred Crl:CD1(ICR) background.

Sox8-EGFP BAC transgenic mice (RRID:MMRRC_031855-UCD) were generated by the GENSAT BAC transgenic project (Gene Expression Nervous System Atlas Project; Gong et al., 2003) and were obtained from the Mutant Mouse Regional Resource Center (MMRRC). Genotyping was performed with either of the following two primer pairs: GFP forward, 5'-AGCAAAGACCCCAACGAGAAGC-3' and GFP reverse, 5'-CCAAACAGATGGCTGGCAAC-3'; or *Sox8-EGFP* forward, 5'-GGTCCCAGAACTGAGACTGAGCTACTG-3', and *Sox8-EGFP* reverse, 5'-GGTCGGGGTAGCGGCTGAA-3'.

Fezf2-TdTomato BAC transgenic mice (RRID:MMRRC_036540-UCD) were generated by the GENSAT BAC transgenic project and were obtained from the MMRRC. Genotyping was performed with the following primers: TdTomato forward, 5'-AGCAAGGGCGAGGAGGTCATC-3'; and TdTomato reverse, 5'-CCTTGGAGC CGTACATGAACTGG-3'.

Isl1^{flx} mice (Mu et al., 2008) were obtained from X. Mu (University of Buffalo, Buffalo, NY) and W. H. Klein (MD Anderson Cancer Center, Houston, TX). Genotyping for both the mutant and wild-type alleles was performed using the following primers (Mu et al., 2008): *Isl1* cKO P1, 5'-TCTCTCATTGGGAAGCAAC-3'; and *Isl1* cKO P2, 5'-TCCA GTGAAGGCCTTCCAGT-3'.

Dlx1-cre BAC mice (RRID:MMRRC_036076-UCD) were generated by the GENSAT BAC transgenic project (Gong et al., 2007) and obtained from the MMRRC. *Foxg1^{IRES-cre}* mice (stock #029690; Kawaguchi et al., 2016) were purchased from The Jackson Laboratory. Both lines were genotyped using the following primers: Cre forward, 5'-GCGGTCTG GCAGTAAAACTATC-3'; and Cre reverse, 5'-CCATGAGTGAA CGAACCTGG-3'.

Fezf2^{PLAP} (MGI:3525887; Chen et al., 2005) mice were obtained from B. Chen (University of California, Santa Cruz, Santa Cruz, CA). Genotyping for this allele was performed using the following two primer pairs (Chen et al., 2005): *Fezf2* mutant forward, 5'-CTGCATGGCTCG GAACGCATCTCC-3', and *Fezf2* mutant reverse, 5'-CACCCCCGG TGAACAGCTCCTCGCCTTGCTCACCAT-3' to detect the mutant allele; and *Fezf2* WT forward, 5'-GAGCCTCAGTTTCTATTCT-3', and *Fezf2* WT reverse, 5'-AGAGAGGGATCTGGCGGGTGAGGTTA TAGTGAGCATTGAACACCTATG-3' to detect the wild-type allele.

Tissue preparation

For the developmental staging of embryos, the morning of the observed vaginal plug was considered as embryonic day 0.5 (E0.5) and the date of birth was considered as postnatal day 0 (P0). Pregnant females were killed by CO₂ asphyxiation, and embryos were removed from the uterus and decapitated. Heads were immersion fixed at 4°C overnight with 4% paraformaldehyde (PFA) in PBS. Fixed heads were rinsed with PBS, removed from the skull, and cryoprotected in 30% sucrose/0.02% sodium azide in PBS. After sinking, brains were either frozen in optimal cutting temperature compound (for coronal sections) or embedded in 7.5% gelatin/20% sucrose in PBS before freezing (for sagittal sections). Samples were sectioned at a thickness of 12 μm on a cryostat, and slides were stored at -20°C.

For postnatal collections, animals were killed by CO₂ asphyxiation. Brains were removed from the skull, immersion fixed in 4% PFA in PBS overnight, rinsed with PBS, and cryoprotected in 20% sucrose/0.02%

sodium azide in PBS. After sinking, brains were sectioned on a freezing sliding microtome at a thickness of 35 μ m. Floating sections were stored short term in 0.3% Triton in potassium PBS (KPBS) at 4°C, and long term in 30% glycerol/30% ethylene glycol in KPBS at –20°C.

Immunohistochemistry

Floating sections were stained before mounting on slides while slide-mounted embryonic sections were processed with solutions added directly to the slide. Standard immunofluorescence and immunohistochemistry using diaminobenzidine (DAB) as a chromogen was conducted as described previously (Waclaw et al., 2006). To summarize, for immunofluorescence, sections were blocked with 2% normal donkey serum (NDS) in KPBS for 1 h, incubated in primary antibody made up in 2% NDS/0.3% Triton in KPBS overnight, incubated in fluorescent secondary antibody made up in 2% NDS/0.3% Triton in KPBS for 2 h, and coverslipped using DAPI Fluoromount-G mountant (catalog #0100–20, SouthernBiotech). For DAB immunohistochemistry, sections were bleached in 0.3% hydrogen peroxide/0.3% Triton in KPBS for 10 min, incubated in primary antibody made up in 2% NDS/0.3% Triton in KPBS overnight, incubated in biotinylated secondary antibody made up in 2% NDS/0.3% Triton in KPBS for 2 h, subjected to an avidin–biotin complex (ABC) binding step using an ABC peroxidase kit (Vector Laboratories; RRID:AB_2336827), and developed in a solution of 4% DAB/0.012% hydrogen peroxide/0.03% Triton in KPBS. Sections were dehydrated and coverslipped using DPX mountant (catalog #06522, Sigma-Aldrich). For both immunofluorescence and DAB immunohistochemistry, all steps were conducted at room temperature. Sections were washed in between incubation steps with either KPBS (cryosections) or 0.3% Triton in KPBS (floating sections). For detecting PLAP (placental alkaline phosphatase) activity, slides were washed for 30 min at 65°C in PBT (0.1% Tween-20 in PBS), for 15 min in room temperature NTMT buffer (Alkaline phosphatase buffer; 100 mM NaCl/100 mM Tris-HCl pH 9.5/50 mM MgCl₂ in PBT), and developed using BM Purple (catalog #11442074001, Roche).

Double staining for Nkx2.1 and Ebf1 was performed using tyramide signal amplification to detect highly (12 \times) dilute rabbit anti-Ebf1 and to quench before visualizing rabbit anti-Nkx2.1 (Chapman et al., 2018). Briefly, sections were bleached in 0.3% hydrogen peroxide/0.3% Triton in KPBS for 10 min and incubated in Ebf1 primary antibody (1:12,000) made up in 2% NDS/0.3% Triton in KPBS overnight. The signal was detected using an Alexa Fluor 488 tyramide signal amplification kit (catalog #T20932, Thermo Fisher Scientific), effectively quenching the primary antibody. Sections were then stained with Nkx2.1 antibody (1:500) following the standard immunofluorescence protocols described above.

The following primary antibodies were used at the indicated dilutions: chicken anti-GFP (1:1000; Aves Laboratories; RRID:AB_10000240); rabbit anti-dsRed (1:1000; Takara Bio; RRID:AB_10013483); rabbit anti-Ebf1 (1:12,000; Millipore; RRID:AB_2636856); rabbit anti-Foxp2 (1:5000; Abcam; RRID:AB_2107107); rabbit anti-Foxp4 (1:100; Abcam; RRID:AB_732431); guinea pig anti-DARPP-32 (1:1500; Synaptic Systems; RRID:AB_2721081); goat anti-Isl1 (1:500; R&D Systems; RRID:AB_2126324); rabbit anti-Isl1 (1:2000; a gift from T. Edlund, Umeå University, Umeå, Sweden); goat anti-mCherry (1:1000; Biorbyt; RRID:AB_2687829); goat anti-Netrin-1 (1:1500; catalog #AF1166SP, R&D Systems); rabbit anti-Nexilin (1:1000; catalog #AB233267, Abcam); rabbit anti-Nkx2.1 (1:500; Seven Hills Bioreagents RRID:AB_451727), and rabbit anti-Zfhx3 (1:1000; MBL International; RRID:AB_10598330).

For immunofluorescence staining, the following fluorescent secondary antibodies from Jackson ImmunoResearch were used (all at 1:500): Alexa Fluor 488-conjugated donkey anti-chicken (RRID:AB_2340375); Alexa Fluor 488-conjugated donkey anti-guinea pig (RRID:AB_2340472); Alexa Fluor 594-conjugated donkey anti-goat (RRID:AB_2340434); Alexa Fluor 594-conjugated donkey anti-rabbit (RRID:AB_2340622); Alexa Fluor 647-conjugated donkey anti-goat (RRID:AB_2340436); and Alexa Fluor 647-conjugated donkey anti-rabbit (RRID:AB_2340625).

For immunohistochemical staining, the following biotinylated secondary antibodies were used (all at 1:500): biotin-conjugated horse anti-

goat (Vector Laboratories; RRID:AB_2336123); biotin-SP-conjugated donkey anti-guinea pig (Jackson ImmunoResearch; RRID:AB_2340451); and biotin-conjugated swine anti-rabbit (Agilent; RRID:AB_2737292).

In situ hybridization

The primers used to generate RNA probes are listed below. Primer sequences were obtained from GenePaint (Visel et al., 2004) and the *Allen Mouse Brain Atlas* (Lein et al., 2007), as indicated. The promoter sequences for T3 polymerase (5'-GCAATTAACCCCTCACTAAAGGG AAC-3') and T7 polymerase (5'-CGTAATACGACTCACTATAGGG CGA-3') were placed at the 5' end of the forward and reverse primers, respectively, to allow for the generation of both antisense and sense (negative control) probes. Probes were generated as described previously (Hua et al., 2018) using a cDNA template generated from E15.5 mouse brain tissue by means of a reverse transcriptase kit (catalog #18091050, Thermo Fisher Scientific). *In situ* hybridization was performed as previously described (Muraleedharan et al., 2021), excepting the substitution of NBT (nitro blue tetrazolium)/BCIP (5-bromo-4-chloro-3-indolyl phosphate; catalog #11681451001, Roche) for BM Purple. A hybridization temperature of 65°C and a dilution of 1:100 were used for all probes.

Cadm2. The following primer sequences were obtained from GenePaint (Set ID EH3798): *Cadm2* forward, 5'-CTGTACCATCCA TAATGCAGGA-3'; and *Cadm2* reverse, 5'-TGTCTCAAAATTGTG CCTAC-3'.

Cntn5. The following primer sequences were obtained from the *Allen Mouse Brain Atlas* (Probe ID RP_060215_01_A11): *Cntn5* forward, 5'-GCCTTTCAGCCAGATCGTAG-3'; and *Cntn5* reverse, 5'-GGAGAGAGAGTGCAGGGTTG-3'.

Grik2. The following primer sequences were obtained from GenePaint (Set ID EH2940): *Grik2* forward, 5'-GTGGCGTAAATA TGACAGGGTT-3'; and *Grik2* reverse, 5'-CAATTAGCTCACGAA CCATTC-3'.

Serpine2. The following primer sequences were obtained from the *Allen Mouse Brain Atlas* (probe ID RP_050614_01_F06): *Serpine2* forward, 5'-TGTGTTTCAGTGTGAAGTGCAG-3'; and *Serpine2* reverse, 5'-TGCCTCACTTAACTGCTGCTAT-3'.

Imaging and image analysis

Images were captured using a Ti-2 SpectraX wide-field microscope (Nikon) or a BX51 microscope (Olympus) equipped with epifluorescence. Images were processed in Adobe Photoshop (Adobe Systems) to optimize brightness/contrast and to pseudocolor images.

RNA sequencing

Dams were killed by CO₂ asphyxiation and E18.5 embryos were dissected from the uterus in cold PBS. Bilateral tissue pieces of LGE/striatum were dissected out and stored in RNAlater (catalog #AM7020, Thermo Fisher Scientific) overnight at 4°C before being moved to –20°C. RNA extraction, RNA quality analysis, and directional poly A RNA sequencing (RNA-seq) were conducted by the University of Cincinnati (Cincinnati, OH) Genomics, Epigenomics, and Sequencing Core (GESC) as previously described (Walsh et al., 2019; Rapp et al., 2020). Briefly, a bioanalyzer (model 2100 Bioanalyzer Instrument, Agilent; RRID:SCR_018043) was used to confirm RNA quality. Poly A RNA was isolated from 1 μ g of total RNA using the NEBNext Poly(A) mRNA Magnetic Isolation Module (catalog #E7490, New England BioLabs) and enriched using the Apollo NGS Library Prep System (catalog #640078, Takara Bio). The library was prepared using the NEBNext Ultra II Directional RNA Library Prep kit (catalog #E7760, New England BioLabs) and quantified with the NEBNext Library Quant kit (catalog #E7630, New England BioLabs). Following proportional pooling of individually indexed libraries, sequencing (single read, 1 \times 85 bp) was performed using a NextSeq 550 Sequencer (catalog #SY-415–1002, Illumina). The Illumina BaseSpace Sequence Hub was used to generate Fastq files. These sequencing data have been deposited in the National Center for Biotechnology Information Gene Expression Omnibus (Edgar et al., 2002) and are accessible through GEO Series accession number (GSE198385).

Experimental design and statistical analysis

Both male and female mice were used for anatomic analyses at postnatal stages; embryos were not genotyped for sex. No phenotypic differences in axonal tract morphology were observed between males and females at postnatal stages. All described mutant phenotypes were completely penetrant in both embryos and postnatal animals. At least three littermate control and three cKO animals were examined at all indicated time points.

For RNA-seq, four littermate control and four cKO animals of each genotype were used for differential gene expression analysis. RNA-seq reads were aligned to University of California, Santa Cruz (Santa Cruz, CA) mouse genome mm10 using STAR aligner (version 2.5; Dobin et al., 2013). Only uniquely aligned reads were retained for downstream analysis. Read counts for each gene were measured using FeatureCounts in the subread package (version 1.6.2; Liao et al., 2014) with an option, “-s 2 -O -fracOverlap 0.8.” Differential gene expression analysis was performed using EdgeR (Robinson et al., 2010), where RUVseq ($k = 1$; Risso et al., 2014) was applied to account for unwanted variation. Genes with \log_2 fold change (FC) > 0.5 and false discovery rate (FDR) < 0.05 were selected as differentially expressed genes (DEGs). BigWig files were generated in RPM scale for each replicate first in a strand-specific manner. Representative BigWig files were then generated for each genotype by averaging the biological replicates. A volcano plot was generated using VolcanoPlot (Goedhart and Luijsterburg, 2020) using FDR < 0.05 and \log_2 FC > 0.5 cutoffs. A gene ontology (GO) term analysis was performed using GONet (Pomaznoy et al., 2018). GO terms with an adjusted p -value < 0.05 were considered significant. A chord plot linking select DEGs with GO terms was generated using the GOplot R package (Walter et al., 2015).

Integrative analyses were performed between our *Isl1* cKO RNA-seq dataset generated here and previously published datasets. We intersected our *Isl1* cKO RNA-seq dataset with a previously published *Ebf1* cKO RNA-seq dataset, applying cutoffs of FDR < 0.05 and a \log_2 FC > 0.5 to their gene expression results (Tinterri et al., 2018, their Supplementary Data 2) before intersection. We additionally intersected our *Isl1* cKO RNA-seq dataset with a previously published list of *Isl1*-associated genes generated from an *Isl1* ChIP-exo study (Rhee et al., 2016, their Supplementary Table 4).

Results

Developmental time course of ascending and descending axonal trajectories populating the internal capsule and cerebral peduncle

The internal capsule carries descending CFAs and striatonigral (dSPN) axons through the diencephalon and into the midbrain where they form the cerebral peduncle, which runs under the STN and substantia nigra. At rostral levels, ascending TCAs enter the internal capsule and associate with CFAs along their trajectory into layer IV of the cerebral cortex. We first assessed the spatial relationships between these axonal pathways at P21. We visualized striatal projections by staining for DARPP-32 (Anderson and Reiner, 1991) and TCAs by immunostaining for the cell surface marker Netrin-G1a (Nakashiba et al., 2000). To mark CFAs, we made use of *Fezf2-TdTomato* BAC reporter mice. *Fezf2* is known to regulate the fate specification of corticofugal pyramidal neurons in both layer V (i.e., corticosubcerebral axons) and layer VI (i.e., CTAs; Chen et al., 2005; Molyneux et al., 2005; Chen et al., 2008; McKenna et al., 2011). At postnatal stages, DARPP-32 dSPN axons (Fig. 1A) and *Fezf2*-TdTomato CFAs (Fig. 1B) exhibit close associations in caudal regions of the internal capsule and cerebral peduncle (Fig. 1D, arrowhead), while Netrin-G1a TCAs (Fig. 1C) retain close associations with CFAs as they ascend through the striatum (Fig. 1D, arrow). These associations suggest that these tracts may guide one another's trajectories. However, the developmental and spatiotemporal relationships between these major forebrain axonal pathways

within the internal capsule are incompletely described. To address this, we made use of *Sox8-EGFP* BAC reporter mice, which allow for the visualization of dSPNs and their growing axons at embryonic stages (Merchan-Sala et al., 2017), together with the aforementioned *Fezf2-TdTomato* BAC reporter mice (CFAs) and Netrin-G1a labeling (TCAs).

At E12.5, when the earliest mouse SPNs are becoming post-mitotic, *Sox8-EGFP* (dSPN) axons can be observed exiting the striatum (Fig. 1E, arrow). In contrast, *Fezf2*-TdTomato CFAs have not yet crossed the cortical-striatal boundary (Fig. 1F, arrow) and Netrin-G1a-positive TCAs exhibit limited extension with only a small number of fibers crossing the diencephalon-telencephalon boundary (Fig. 1G, arrow). While there is an association of dSPN axons and TCAs within the MGE at this early stage (Fig. 1H, arrow), there are no apparent CFA/dSPN axon or CFA/TCA interactions.

Previous work has shown that pioneer CFAs pause in the subpallium (striatum) from E13.5 to E14.5 until ascending TCAs contact them at approximately E15.5 (De Carlos and O'Leary, 1992; Deck et al., 2013). Their relationship, however, to growing SPN axons, particularly dSPN axons, at this developmental stage has not been examined. We find that a significant portion of *Sox8-EGFP* dSPN axons have extended to their final target in the SNr by E14.5 (Fig. 1I, arrow) while CFAs only extend into the lateral striatum and TCAs have not extended beyond the GP (Fig. 1J,K, arrows). Similar to earlier stages, dSPN axons and TCAs remain closely associated at the level of the GP at E14.5 (Fig. 1L, arrow), but there are still no observable CFA/dSPN axon or CFA/TCA interactions. Striatonigral axons thus precede descending CFAs in coursing through the diencephalon and midbrain, defining the ultimate route of the internal capsule/cerebral peduncle.

Further elaboration of *Sox8-EGFP* dSPN axons along the forming internal capsule/cerebral peduncle is apparent by E16.5, together with terminal arborization within the SNr (Fig. 1M, arrow). At this stage, many CFAs have extended through the diencephalon and midbrain (Fig. 1N, arrow), and into the hindbrain (data not shown). Furthermore, TCAs have reached the cerebral cortex by this stage (Fig. 1O, arrow), thereby establishing the trajectories of all three pathways between the cortex and midbrain (Fig. 1P). To better define the spatial relationships and associations between each pathway, we examined high-power images at both rostral (Fig. 1Q–S, solid box in P) and caudal (Fig. 1T–V, dotted box in P) levels. At more rostral levels, CFAs form close associations with TCAs (Fig. 1S, arrow), which are less apparent with dSPN axons (Fig. 1Q, arrowhead). Despite the close association of TCAs and dSPN axons at the level of the GP (Fig. 1U, arrow), there is little overlap between these axons within the striatum (Fig. 1R, arrowhead). As CFAs destined for targets in the brainstem and spinal cord (i.e., corticosubcerebral axons) extend caudal to the GP, they diverge from the already established trajectories of ascending TCAs (Fig. 1V, open and solid arrowheads). Thus, while descending caudally, CFAs appear to exchange their associations with TCAs for those with dSPN axons, coursing instead alongside the striatonigral axons that preceded them into the posterior internal capsule/cerebral peduncle (Fig. 1T, open arrow). This apparent handoff suggests that pioneering dSPN axons may guide descending CFAs as they travel beyond the GP. This is in line with previous observations that both the striatopallidal junction and the MGE-derived GP serve as intermediate/choice point regions important for CFA and TCA pathfinding (Métin and Godement, 1996; Marín et al., 2002; Kaur et al., 2020).

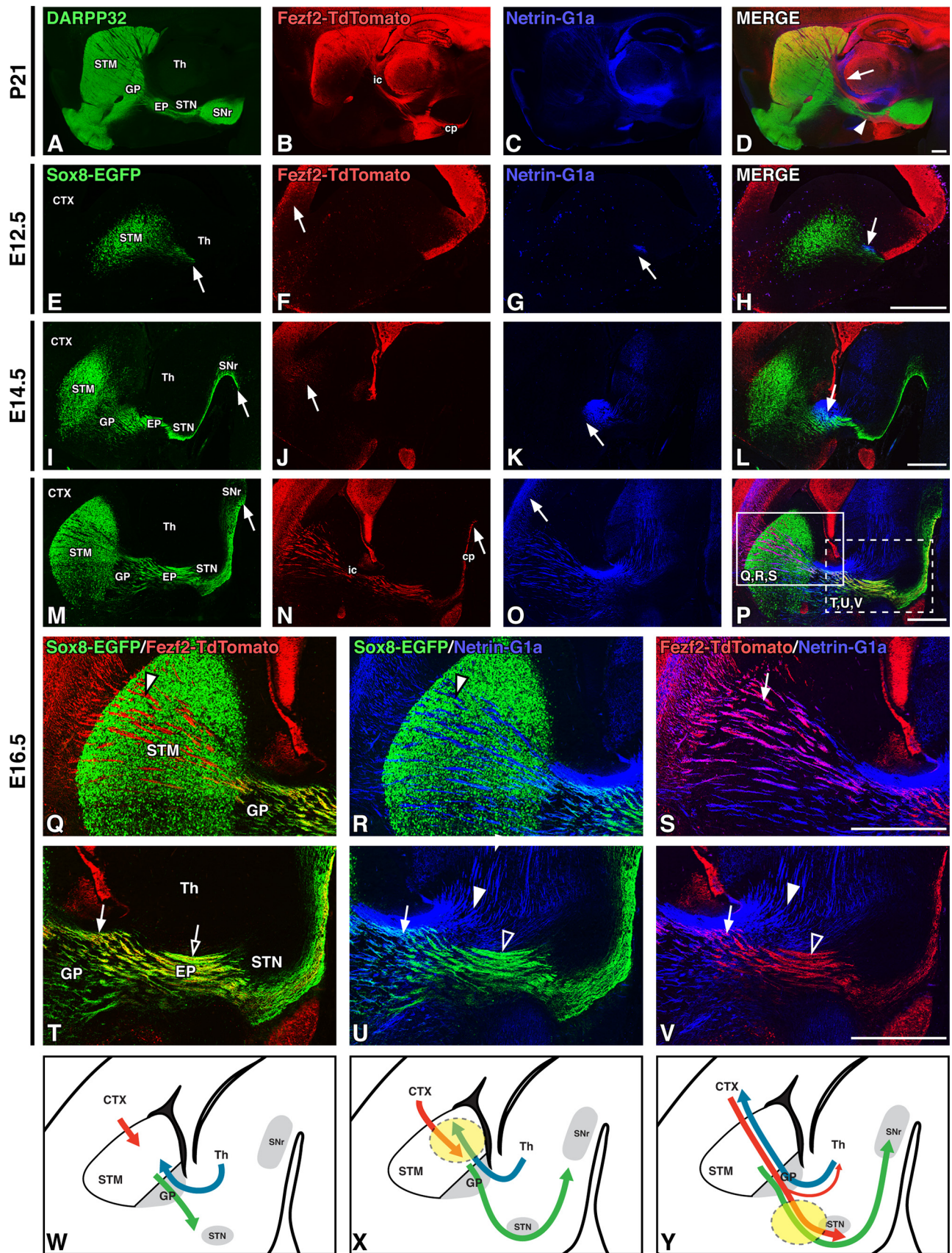


Figure 1. Striatal direct pathway axons pioneer the forming internal capsule/cerebral peduncle. **A–D**, DARPP-32 labeling of striatal projections (**A**), Fezf2-TdTomato labeling of corticofugal pathway axons (**B**), Netrin-G1a labeling of thalamocortical axons (**C**), and merged labeling (**D**) in sagittal P21 *Fezf2-TdTomato* BAC transgenic mouse brain sections shows the normal spatial relationships between internal capsule/striatum, corticofugal, and thalamocortical axon outgrowth in sagittal sections of *Sox8-EGFP*; *Fezf2-TdTomato* BAC transgenic mouse brains from E12.5 to E16.5, with *Sox8-EGFP* labeling of striatal direct pathway axons (**E**, **I**, **M**), Fezf2-TdTomato labeling (**F**, **J**, **N**), Netrin-G1a labeling (**G**, **K**, **O**), and merged

Together, these developmental observations show that the spatial relationships defining the internal capsule/cerebral peduncle at postnatal stages are established by late embryonic stages. Most importantly, our data show that striatonigral axons are early populators of the forming internal capsule/cerebral peduncle and that the forming direct pathway is thus well positioned to guide descending cortical projections (i.e., CFAs) and ascending thalamic projections (i.e., TCAs) within this major forebrain axon tract. The spatiotemporal dynamics of axonal trajectories within the developing internal capsule/cerebral peduncle are summarized in Figure 1W–Y.

Altered axon trajectories within the internal capsule/cerebral peduncle of postnatal *Isl1* cKOs

Given that striatonigral axons are the earliest occupants of the forming internal capsule/cerebral peduncle, we set out to determine whether alterations in their development lead to secondary effects on the axonal trajectories of CFAs and TCAs. The LIM-homeodomain transcription factor *Isl1* is expressed in dSPNs and is required for the survival and differentiation of early-born striatonigral neurons (Ehrman et al., 2013; Lu et al., 2014; Merchan-Sala et al., 2017; Waclaw et al., 2017). Conditional *Isl1* inactivation (i.e., cKO) within the ventral forebrain results in a smaller striatum, disorganized striatonigral projections, and reduced dSPN innervation of the SNr. In addition to the aberrant dSPN axons observed in the *Isl1* cKOs, a more general disruption of the internal capsule/cerebral peduncle has been described using neurofilament staining (Ehrman et al., 2013) suggesting alterations in CFA trajectories. Importantly, although *Isl1* is also expressed in additional telencephalic (e.g., cholinergic) and diencephalic (e.g., reticular thalamic and hypothalamic) neurons (Thor et al., 1991; López-Bendito et al., 2006; Siddiqi et al., 2021), this factor is not expressed in either corticofugal or thalamocortical projection neurons.

To conditionally inactivate striatal *Isl1* expression, we crossed an *Isl1^{flx/flx}* mouse line, wherein exon 3 containing the second LIM domain is flanked by loxP sites (Mu et al., 2008), with a *Dlx1-cre* BAC mouse line that drives Cre-mediated recombination in the vast majority of ventral forebrain neuronal progenitors (Gong et al., 2007; Taniguchi et al., 2011; Gerfen et al., 2013). This driver thus targets *Isl1*-positive populations within both the subpallium (e.g., striatal neuron populations) and the diencephalon (including reticular thalamic and hypothalamic neuronal populations). To simultaneously label CFAs, we crossed the *Fezf2-TdTomato* BAC reporter onto the *Isl1* cKOs.

←

labeling (H, L, P). Arrows indicate the farthest extent of axon outgrowth and illustrate that direct pathway axons precede corticofugal and thalamocortical pathway entry into the forming internal capsule. Q–V, High-power images of E16.5 sections at rostral (Q, R, S; P, solid box) and caudal (T, U, V; P, dotted box) levels. Sox8-EGFP/*Fezf2-TdTomato* (Q, T), Sox8-EGFP/*Netrin-G1a* (R, U), and *Fezf2-TdTomato*/*Netrin-G1a* (S, V) double-labeling of direct pathway axons (green), descending corticofugal axons (red), and ascending thalamocortical axons (blue). Arrowheads indicate single-labeled tracts, and arrows indicate double-labeled/closely associated tracts. All three tracts are closely associated at the GP (T, U, V, arrows). Corticofugal axons have close associations with thalamocortical axons rostrally (S, arrow) but diverge from them (V, arrowheads) and instead travel with striatal direct pathway axons as they descend caudal to the GP (T, open arrow). W–Y, Cartoon diagrams of striatal direct pathway (green), corticofugal (red), and thalamocortical (blue) outgrowth over time illustrating early striatal direct pathway entry into the internal capsule (W) and a proposed handoff of descending corticofugal axons from ascending thalamocortical axons (X, dashed circle) to striatal direct pathway axons (Y, dashed circle). cp, Cerebral peduncle; CTX, cortex; ic, internal capsule; STM, striatum; Th, thalamus. Scale bars, 500 μ m.

We first analyzed relationships among SPN axons, CFAs, and TCAs in the mature internal capsule/cerebral peduncle of postnatal *Isl1* cKOs (*Dlx1-cre; Isl1^{flx/flx}; Fezf2-TdTomato*) and littermate controls (*Dlx1-cre; Isl1^{flx/+}; Fezf2-TdTomato* or *Isl1^{flx/flx}; Fezf2-TdTomato*). As reported previously (Ehrman et al., 2013), DARPP-32-positive striatal axons exhibit a reduced and disorganized appearance within the internal capsule/cerebral peduncle of the *Isl1* cKOs (Fig. 2I,K,L) compared with controls (Fig. 2A,C,D). Notably, the DARPP-32-positive striatonigral axons that course underneath the STN in controls (Fig. 2D, solid arrowhead) pass directly through the STN in *Isl1* cKOs (Fig. 2L, solid arrowhead). Interestingly, the *Fezf2-TdTomato* CFAs show similar defects to the striatal axons within the internal capsule/cerebral peduncle of *Isl1* cKOs (Fig. 2, compare J–M, B–E). In particular, CFAs are observed to be defasciculated, as evidenced by the numerous axon bundles passing through the STN (Fig. 2E,M, marked by Foxp2) of *Isl1* cKOs (Fig. 2L,M) compared with coalescing tightly with dSPN axons and running underneath the STN in controls (Fig. 2D,E). Furthermore, unlike control animals where the CFAs remain fasciculated within the cerebral peduncle underneath the SNr (Fig. 2B–D), the defasciculated CFAs in *Isl1* cKOs course directly from the STN through the dorsal half of the SNr, such that these mutants essentially lack a cerebral peduncle (Fig. 2J–L). Coronal sections further illustrate the defasciculation and increased ventral spread of CFAs in the anterior portion of the internal capsule of *Isl1* cKOs compared with controls (Fig. 2F,N, arrows). CFAs in *Isl1* cKOs also remain on abnormal trajectories posterior to the SNr, taking a more dorsal route through the hindbrain (Fig. 2G,O, arrows), indicating that corticosubcerebral axons are unable to recover their normal trajectories in *Isl1* cKOs even after extending caudal to their associations with the mutant striatonigral fibers. Importantly, these CFA defects observed in *Isl1* cKOs occur despite the fact that cortical projection neurons do not express *Isl1*, further implicating striatonigral axons as pioneers that guide and organize CFAs within the internal capsule/cerebral peduncle. Summaries of these control and *Isl1* mutant CFA (red) and striatonigral axon (green) trajectories are diagrammed in Figure 2, H and P.

As described above, growing TCAs contact dSPN axons more than 2 d before contacting the descending CFAs. Accordingly, *Isl1* cKOs also exhibit a disrupted relationship between the striatonigral and thalamocortical pathways at postnatal stages, although the TCA defects are less severe than those described above for mutant CFAs. To better visualize this relationship, we examined images of P21 sagittal brain sections at a more medial level than shown in Figure 2. At this level, the reduction of DARPP-32-positive striatal axons projecting to the SNr in *Isl1* mutants is even more apparent (Fig. 3, compare A, G at arrows). While *Netrin-G1a*-positive TCAs can be observed extending to their final targets within the cortex in *Isl1* cKOs, disorganization within these ascending fibers is present within the rTh and GP, where mutant fibers can be observed deviating ventrally in both sagittal (Fig. 3, compare H, B at arrows) and coronal (Fig. 3, compare K, E at arrows) planes. Merged labeling of DARPP-32-positive striatal projections and *Netrin-G1a*-positive TCAs demonstrate that TCA disorganization is most appreciable just posterior to the termination of DARPP-32-positive striatopallidal fibers—intact in *Isl1* mutants—within the GP (Fig. 3C,D). High-power images further illustrate the location of striatonigral and TCA defects (Fig. 3D,J, boxes in C,I); mutant TCAs are tangled and disorganized as they ascend past the GP (Fig. 3, compare D, J at arrowheads). This region is also where the reduction of DARPP-32-positive striatonigral fibers becomes most noticeable (Fig. 3, compare D, J at arrows). These findings suggest that early

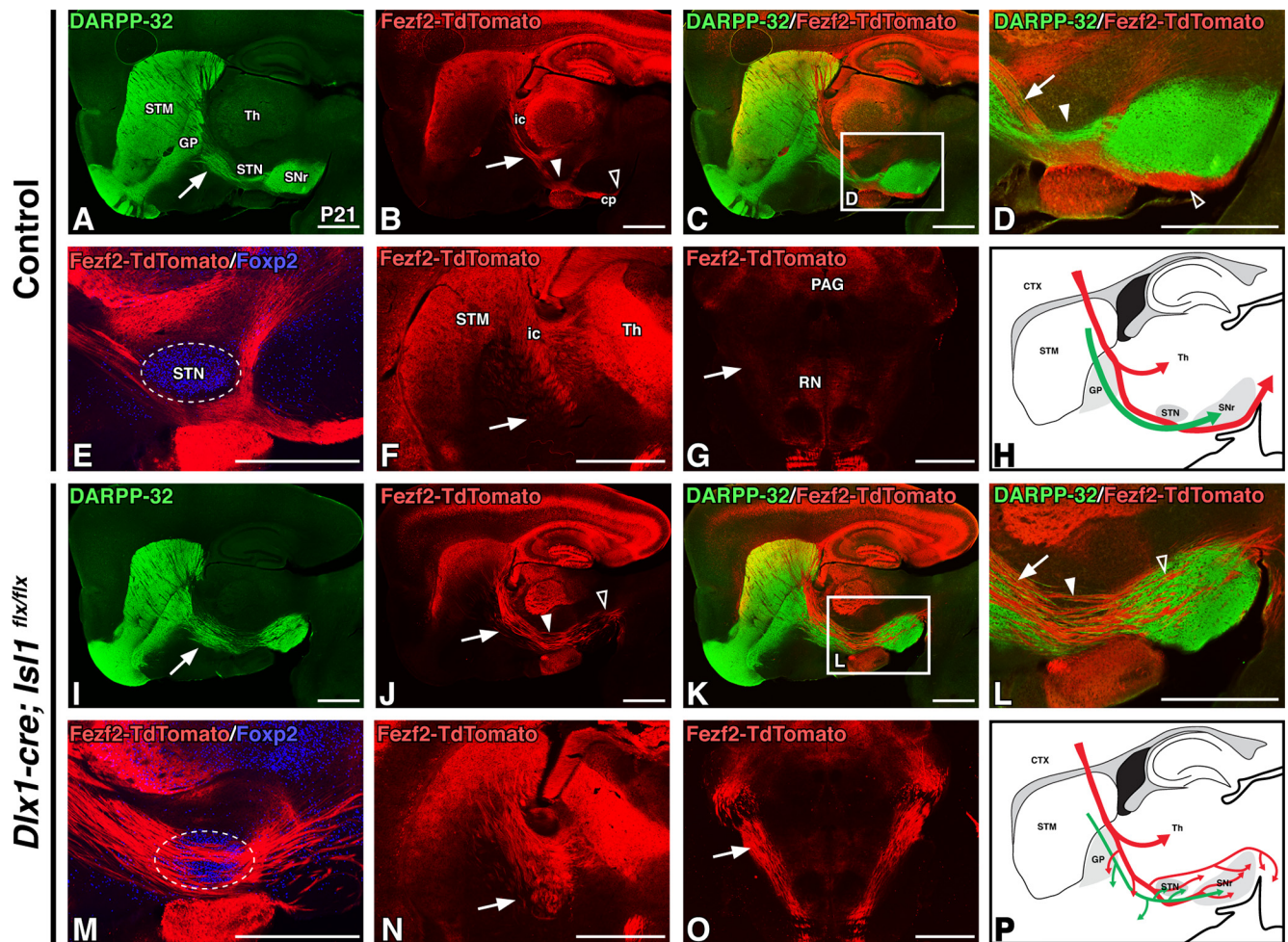


Figure 2. Conditional loss of *Isl1* within the ventral forebrain results in postnatal corticofugal axon defects. **A–E, I–M**, Sagittal sections of P21 control (*Dlx1-cre; Isl1^{flx/+}; Fezf2-TdTomato* or *Isl1^{flx/flx}; Fezf2-TdTomato*, $n = 3$; **A–E**) and *Isl1* cKO (*Dlx1-cre; Isl1^{flx/flx}; Fezf2-TdTomato*, $n = 3$; **I–M**) transgenic mouse brains. DARPP-32 labeling of striatal projections (**A, I**), Fezf2-TdTomato labeling of corticofugal axons (**B, J**), DARPP-32/Fezf2-TdTomato double-labeling at low power (**C, K**), DARPP-32/Fezf2-TdTomato double-labeling at high power (**D, L**; **C, K**, boxes) and Fezf2-TdTomato/Foxp2 (STN marker, boundaries outlined) double-labeling (**E, M**). Striatal projections (green) are disorganized in *Isl1* cKOs (**A, I**, arrows). Corticofugal axons (red) defasciculate, exhibit ventral deviation (**B, D, J, L**, arrows), override the STN (**E, M**; **B, D, J, L**, solid arrowheads), and take aberrant paths through the cerebral peduncle (**B, D, J, L**, open arrowheads). **F, G, N, O**, Fezf2-TdTomato labeling in P21 coronal sections of control (**F, G**, $n = 3$) and *Isl1* mutants (**N, O**, $n = 3$) at rostral (**F, N**) and caudal (**G, O**, pseudocolored DAB immunohistochemical staining) levels further illustrate disorganization, ventral misrouting (**F, N**, arrows), and aberrant trajectories of corticospinal axons at the pontine level (**G, O**, arrows). **H, P**, Cartoon diagrams illustrating a sagittal view of altered direct pathway (green) and corticofugal pathway (red) axon trajectories in adult *Isl1* cKOs (**P**) compared with controls (**H**). cp, Cerebral peduncle; CTX, cortex; ic, internal capsule; PAG, periaqueductal gray; RN, red nucleus; STM, striatum; Th, thalamus. Scale bars, 1000 μm .

interactions (i.e., E12.5) between striatal axons and TCAs as they first enter the internal capsule at these rostral regions could contribute to the normal assembly of thalamocortical projections. Control and *Isl1* mutant TCA (blue) and striatonigral axon (green) trajectories are summarized in Figure 3, *F* and *L*.

In summary, our postnatal observations of *Isl1* cKOs show that, despite not being expressed in either corticofugal or thalamocortical projection neurons, the loss of ventral forebrain *Isl1* expression can drive CFA and, to a lesser extent, TCA defects. Overall, these data suggest a direct role for the pioneering striatonigral axons in the guidance of CFAs and TCAs, with the extension of CFAs past the guidance populations located within the GP being particularly sensitive to defects in striatonigral axon outgrowth.

Diencephalic *Isl1* neuronal populations bound internal capsule/cerebral peduncle axon trajectories during development

We next sought to examine the developmental origin of the internal capsule pathway defects observed in postnatal *Isl1* cKOs.

In doing so, we also wanted to design a conditional knock-out strategy that would allow us to distinguish between axon guidance contributions from those *Isl1*-positive populations located outside of the striatum and those located within the striatum. This is important because, in addition to being expressed in dSPNs, *Isl1* is also expressed within forebrain cholinergic interneuron populations, lateral ganglionic eminence (LGE)-derived corridor cells positioned within the MGE, prospective melanocytic neurons of the hypothalamus (Hyp), the hypothalamic arcuate nucleus, the reticular thalamic nucleus (rTh), and the zona incerta (Thor et al., 1991; López-Bendito et al., 2006; Bielle et al., 2011b; Nasif et al., 2015; Feng et al., 2016; Siddiqi et al., 2021).

At E18.5, *Isl1*-positive populations within the rTh and Hyp border the axons of the forming internal capsule and cerebral peduncle. Both DARPP-32-positive striatal projections and Fezf2-TdTomato-positive CFAs pass between these two diencephalic *Isl1* populations (Fig. 4*A, B*, arrowheads). In contrast, the rTh is a permissive region for both descending CFAs and

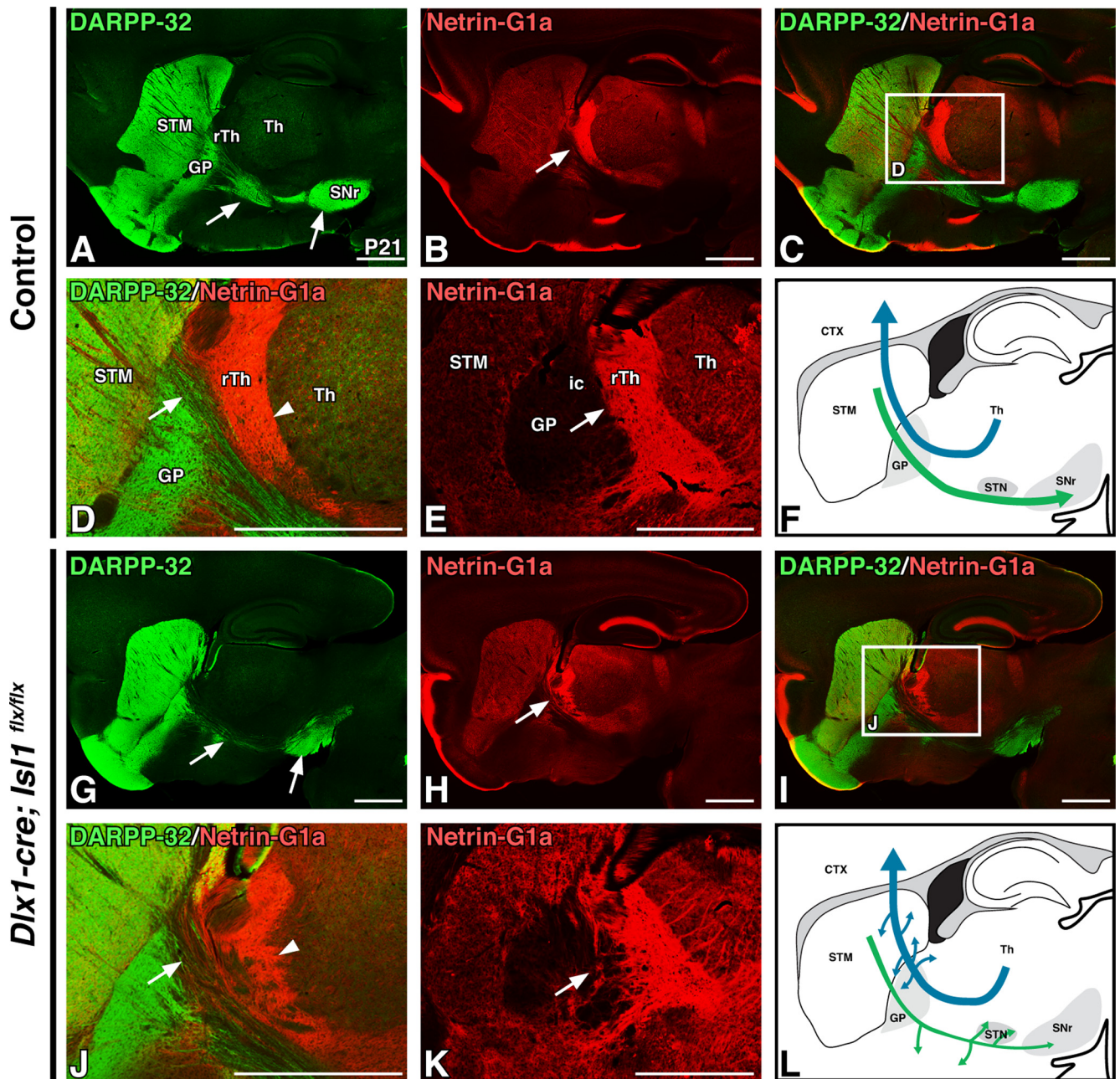


Figure 3. Conditional loss of *Is11* within the ventral forebrain results in subtle postnatal thalamocortical axon defects. **A–D, G–J**, Sagittal sections of P21 control (*Dlx1-cre; Is11^{fix/+}; Fezf2-TdTomato*) or *Is11^{fix/fix}; Fezf2-TdTomato*, $n = 3$; **A–D**) and *Is11* cKO (*Dlx1-cre; Is11^{fix/fix}; Fezf2-TdTomato*, $n = 3$; **G–J**) transgenic mouse brains. DARPP-32 labeling is shown of striatal projections (**A, G**), Netrin-G1a labeling of thalamocortical axons (**B, H**), and merged labeling at low (**C, I**) and high (**D, J**; **C** and **I**, boxes) power. Thalamocortical axons (red) exhibit mild disorganization dorsal to the GP (**B, D, H, J**, arrowheads). **E, K**, Pseudocolored Netrin-G1a DAB immunohistochemical staining in P21 coronal sections from control (**E**; $n = 3$) and *Is11* cKOs (**K**; $n = 3$) further exemplifies thalamocortical projection abnormalities. **F, L**, Cartoon diagrams illustrating a sagittal view of altered direct pathway (green) and thalamocortical pathway (blue) axon trajectories in postnatal *Is11* cKOs (**L**) compared with controls (**F**). CTX, Cortex; ic, internal capsule; STM, striatum; Th, thalamus. Scale bars, 1000 μm .

ascending TCAs to traverse as they cross the telencephalon-diencephalon boundary (Fig. 4B,C, solid arrowheads). Finally, TCAs run rostral to, and do not interact with, the *Is11*-positive populations located within the Hyp (Fig. 4C, open arrowhead).

Is11 populations within the rTh and Hyp are thus well placed to guide axon trajectories through the internal capsule. As these diencephalic populations lose their *Is11* expression in our *Dlx1-cre* driven *Is11* cKOs, we cannot rule out the possibility that defects within these populations contribute to the observed axon abnormalities in mutants. Therefore, to test the idea that it is striatonigral axon defects rather than diencephalic defects driving these phenotypes, we generated and analyzed two separate

Is11 cKO lines—one for which *Is11* loss is ventral forebrain specific (i.e., subpallium and diencephalon; *Dlx1-cre* driver) and one for which *Is11* loss is telencephalon specific (i.e., pallium and subpallium; *Foxg1^{IRRES-cre}* driver). When compared with control *Is11* expression at E18.5 (Fig. 4D), ventral forebrain-specific inactivation of *Is11* via *Dlx1-cre* largely removes *Is11* expression from the striatum, rTh, and Hyp (Fig. 4E). In contrast, the telencephalon-specific *Foxg1^{IRRES-cre}* driver efficiently removes striatal *Is11* (Fig. 4F, arrow) while sparing diencephalic *Is11* expression (Fig. 4F, arrowheads). Comparisons among *Is11* expression in controls, ventral forebrain-specific *Is11* cKOs, and telencephalon-specific *Is11* cKOs are illustrated in Figure 4G–I.

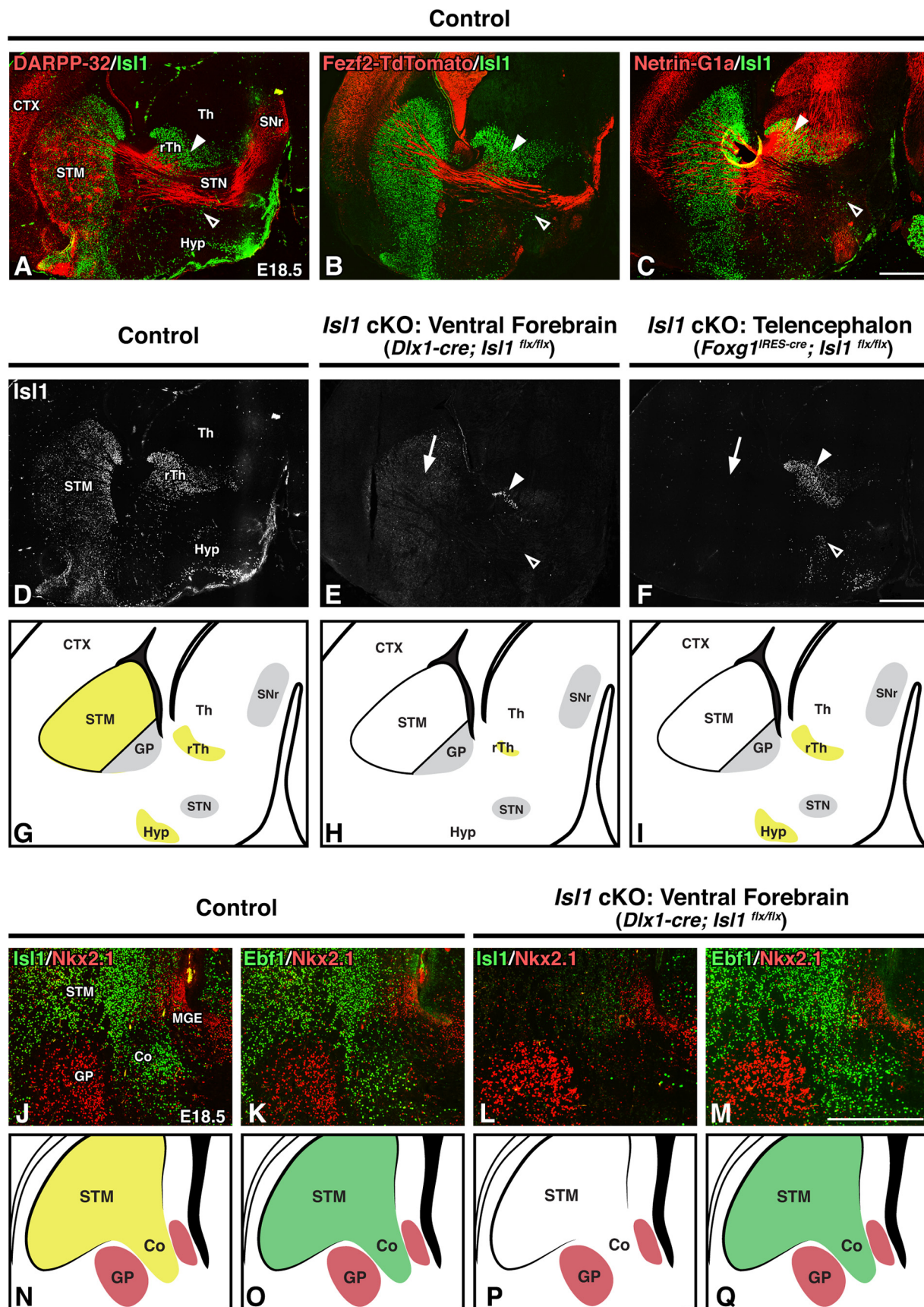


Figure 4. Telencephalon-specific inactivation of *Is1* removes *Is1* expression from the STM but spares *Is1* expression within diencephalic populations bordering the internal capsule. **A–F**, Sagittal brain sections of E18.5 controls (*Dlx1-cre; Is1^{flx/+}*; *Fezf2-TdTomato* or *Foxg1^{IRES-cre}; Is1^{flx/+}*; *Fezf2-TdTomato*, $n = 6$; **A–D**), ventral forebrain-specific *Is1* cKOs (*Dlx1-cre; Is1^{flx/flx}*; *Fezf2-TdTomato*, $n = 3$; **E**), and telencephalon-specific *Is1* cKOs (*Foxg1^{IRES-cre}; Is1^{flx/flx}*; *Fezf2-TdTomato*, $n = 3$; **F**). Double-labeling with *Is1* and DARPP-32 to mark striatal projections (**A**), *Fezf2-TdTomato* to mark descending corticofugal projections (**B**), or *Netrin-G1a* to mark ascending thalamocortical projections (**C**). *Is1*-positive populations within the rTh and Hyp (**A**, **B**, **C**,

In addition to these diencephalic populations, *Isl1* is also expressed within a population of LGE-derived GABAergic neurons that migrate tangentially into the MGE by E11.5 (López-Bendito et al., 2006). Termed corridor cells, these neurons serve as guideposts by defining a region between the proliferative MGE and forming GP through which TCAs ascend. Highlighting their role as guideposts, disruption of corridor cell localization and/or function leads to TCA defects (López-Bendito et al., 2006; Simpson et al., 2009; Bielle et al., 2011a, b). As these cells originate in the subpallium, they are impacted by both the *Dlx1-cre* and *Foxg1^{IRRES-cre}* drivers. Indeed, staining for the corridor (visualized as an Nkx2.1-negative region bordered by Nkx2.1-positive MGE/GP populations) in E18.5 coronal sections shows that *Isl1* mutants (*Dlx1-cre*) largely lack *Isl1* expression within these cells (Fig. 4J,L). In addition to *Isl1*, corridor cells are also marked by several other canonical SPN markers including *Ebf1* (López-Bendito et al., 2006). To further assess corridor integrity in *Isl1* cKOs, we stained for *Ebf1* and found that these guidepost cells are appropriately localized within the corridor (Fig. 4K,M). Thus, although we cannot exclude that dysfunction within these cells contributes to the observed axon defects, the mutant corridor is overtly intact. A summary of corridor marker expression in controls and *Isl1* mutants is illustrated in Figure 4N–Q.

Foxg1^{IRRES-cre}; *Isl1^{flx/flx}* animals are born at normal Mendelian ratios but die several days after birth from unknown causes. Germline loss of *Isl1* is lethal by E10.5 because of cardiac defects (Pfaff et al., 1996; Cai et al., 2003), necessitating conditional strategies to examine roles for *Isl1* from mid-gestation into adulthood. Despite this postnatal lethality, we were able to examine pathfinding defects throughout the whole of embryogenesis for this line. Lethality using this strategy is a notable difference from our previous approach using a binary inducible Cre system (*Foxg1^{ITa}*; *TetO-cre*; *Isl1^{flx/flx}*) to delete *Isl1* specifically within the telencephalon (Ehrman et al., 2013). This is likely because of inefficiencies in the multistep tTA/TetO system to induce Cre, which allows for postnatal survival.

Embryonic defects in the formation of the internal capsule/cerebral peduncle using ventral forebrain-specific or telencephalon-specific inactivation of *Isl1*

To examine how defective striatonigral axon outgrowth influences CFA and TCA pathfinding during development, we analyzed the spatial relationships among striatal, corticofugal, and thalamo-cortical projections in both ventral forebrain-specific (*Dlx1-cre*; *Isl1^{flx/flx}*; *Sox8-EGFP*; *Fezf2-TdTomato*) and telencephalon-specific (*Foxg1^{IRRES-cre}*; *Isl1^{flx/flx}*; *Sox8-EGFP*; *Fezf2-TdTomato*) *Isl1* cKO embryos. Heterozygous littermates (*Dlx1-cre*; *Isl1^{flx/+}*; *Sox8-EGFP*;

Fezf2-TdTomato or *Foxg1^{IRRES-cre}*; *Isl1^{flx/+}*; *Sox8-EGFP*; *Fezf2-TdTomato*) served as controls.

Both of these *Isl1* cKO lines exhibit highly similar dSPN and CFA malformations, largely identical to those seen in the postnatal *Isl1* mutants described above, when assessed at E18.5. For example, dSPN axons are defasciculated, override the STN, and remain disorganized as they reach the SNr in both *Isl1* mutants (Fig. 5A,H,O). This holds true for CFA malformations as well; compared with controls, the CFAs of both *Isl1* mutants are defasciculated as they traverse the internal capsule, show increased ventral spread (Fig. 5B,I,P, solid arrows), override the STN (Fig. 5B,I,P, solid arrowheads), and take aberrant routes through the SNr, failing to coalesce into a recognizable cerebral peduncle (Fig. 5B,I,P, open arrows). Merged *Sox8-EGFP* and *Fezf2-TdTomato* labeling further demonstrates that the disruption of the normal organization between these two tracts seen in postnatal *Isl1* cKOs originates during embryonic time points (Fig. 5C,J,Q). We next assessed these defects in more detail in high-power images taken at the entopeduncular nucleus (EP; Fig. 5D, K,R, solid boxes in C,J,Q) and cerebral peduncle (Fig. 5E,L,S, dotted boxes in C,J,Q). Forming CFAs normally follow a stereotyped trajectory; as seen at postnatal stages (Fig. 2C,D), CFAs run dorsal to dSPN axons (Fig. 5C,D) before crossing ventral to them as these two tracts approach the STN (Fig. 5C,E). Mutant CFA fibers do not take these stereotyped trajectories. They instead deviate ventrally over dSPN axons (Fig. 5, compare D,K,R at arrows) and course through, rather than around, the SNr (Fig. 5E,L,S). We additionally costained sections for *Foxp2*, which further demonstrates that both striatonigral axons (Fig. 5F,M,T) and CFAs (Fig. 5G,N,U) misroute and pass directly through the STN. Together, both our postnatal and embryonic observations support the notion that intrinsic dSPN axon outgrowth defects in *Isl1* cKOs appear to non-cell autonomously impact CFA trajectories.

One instance for which *Dlx1-cre*- and *Foxg1^{IRRES-cre}*-driven *Isl1* cKOs do differ is with regard to CTA trajectories; an increased number of CFAs are observed routing to the thalamus in ventral forebrain-specific (*Dlx1-cre*), but not in telencephalon-specific (*Foxg1^{IRRES-cre}*), *Isl1* cKOs (Fig. 5, compare B,I,P at open arrowheads). The likely reason for this difference is that *Isl1* is lost from the diencephalon (e.g., rTh) of the *Dlx1-cre*, but not the *Foxg1^{IRRES-cre}*, *Isl1* cKOs. Defects within the rTh may permit descending cortical projections originally destined for subcerebral targets (i.e., corticosubcerebral axons) to instead aberrantly route through the rTh into the thalamus. Notably, this phenotype was not observed in postnatal *Dlx1-cre Isl1* cKOs, perhaps indicating that the aberrant axons that are misrouted into the thalamus do not find appropriate targets and are subsequently pruned. Embryonic control and *Isl1* cKO CFA (red) and striatonigral (green) axon trajectories are summarized in Figure 5V–X.

We additionally examined both ventral forebrain- and telencephalon-specific *Isl1* cKOs for TCA defects at embryonic stages. Both of these knock-out strategies result in largely identical TCA defects, and, as seen postnatally, these defects are less severe than those observed for CFAs. Netrin-G1a-positive TCAs can be seen making it to their final targets in the cortex (Fig. 6A–C, arrows), but are disorganized as they ascend. High-power views at the level of the GP (Fig. 6D–I, boxes in A–C) illustrate that, as was observed postnatally (Fig. 3), both mutants exhibit TCAs that are disorganized and tangled ventrally around the GP when compared with controls (Fig. 6D–I, arrowheads). Furthermore, TCAs are defasciculated and reduced in number as they ascend to the cortex (Fig. 6D–I, arrows). As with CFAs, the presence of these

←

arrowheads) border axon projections as they extend through the internal capsule/cerebral peduncle. *Isl1* single-labeling (D, E, F) shows that both *Dlx1-cre* and *Foxg1-cre* drivers delete *Isl1* expression in the STM (E, F, arrows), but only the *Dlx1-cre* driver efficiently removes *Isl1* expression from the Hyp (E, F, open arrowheads) and rTh (E, F, solid arrowheads). G–I, Cartoon diagrams comparing *Isl1* expression (yellow) in controls (G), ventral forebrain-specific *Isl1* cKOs (H), and telencephalon-specific *Isl1* cKOs (I). J–M, Coronal brain sections of E18.5 controls (*Dlx1-cre*; *Isl1^{flx/+}*, *n* = 3; J, K) and ventral forebrain-specific *Isl1* cKOs (*Dlx1-cre*; *Isl1^{flx/flx}*, *n* = 3; L, M). Double-labeling with GP marker Nkx2.1 and either *Isl1* (J, L) or *Ebf1* (tyramide amplified; K, M) shows that corridor cells are appropriately located in *Isl1* mutants. N–Q, Cartoon diagrams comparing *Isl1* (N, P, yellow) and *Ebf1* (O, Q, green) expression in controls (N, O) and ventral forebrain-specific *Isl1* cKOs (P, Q). Co, Corridor; CTX, cortex; STM, striatum; Th, thalamus. Scale bars: A–F, 500 μ m; J–M, 250 μ m.

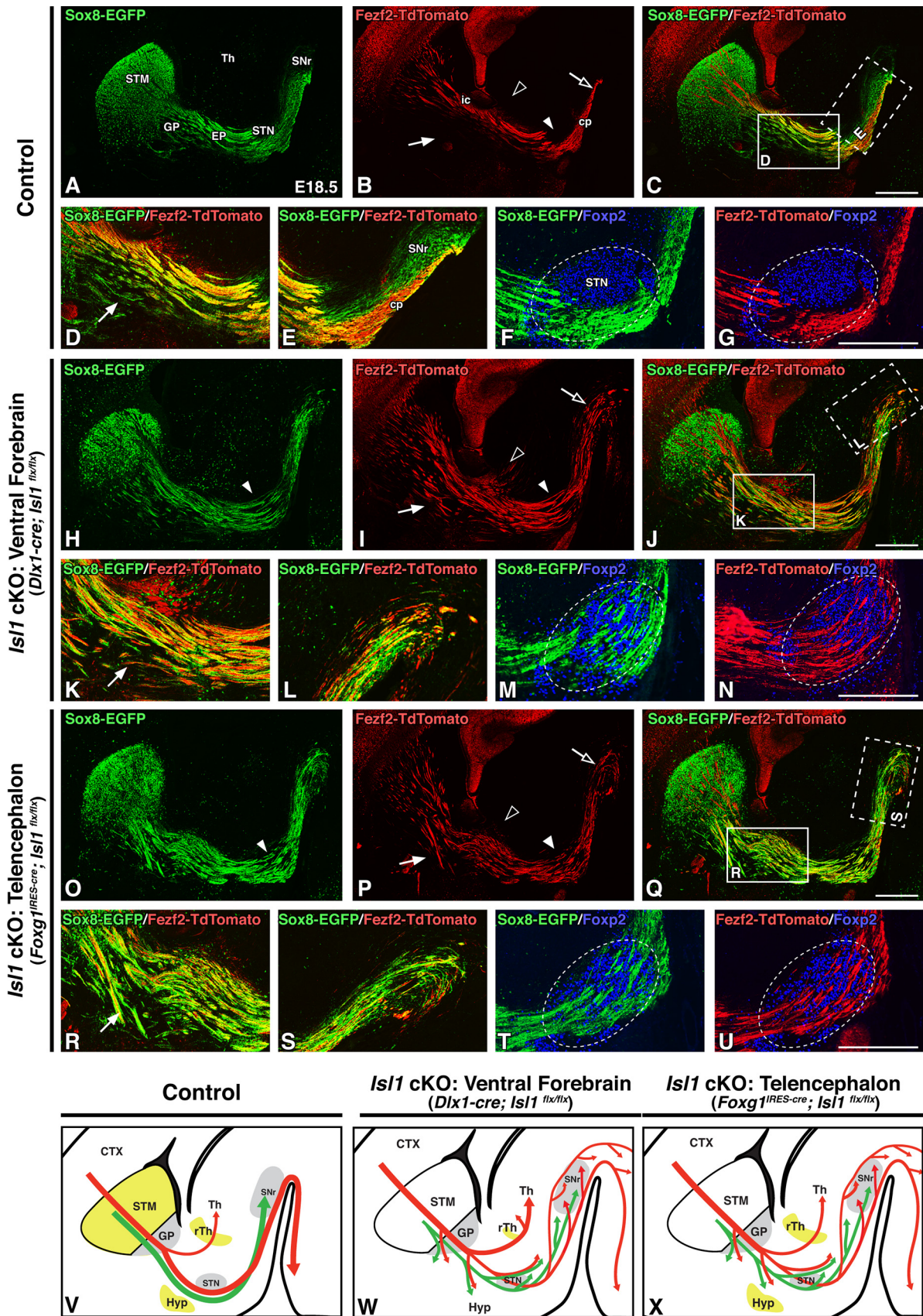


Figure 5. Loss of striatal *Is11* expression is sufficient to drive corticofugal axon defects during embryonic development. **A–U**, Sagittal brain sections of E18.5 control (*Dlx1-cre; Is11^{flx/+}*; Sox8-EGFP; Fezf2-TdTomato or *Foxg1^{IRES-cre}; Is11^{flx/+}*; Sox8-EGFP; Fezf2-TdTomato, *n* = 6; **A–G**), ventral forebrain-specific *Is11* cKOs (*Dlx1-cre; Is11^{flx/flx}*; Sox8-EGFP; Fezf2-TdTomato, *n* = 3; **H–N**), and telencephalon-specific *Is11* cKOs (*Foxg1^{IRES-cre}; Is11^{flx/flx}*; Sox8-EGFP; Fezf2-TdTomato, *n* = 3; **O–U**). Sox8-EGFP labeling of striatal direct pathway axons (**A**, **H**, **O**), Fezf2-TdTomato labeling of corticofugal pathway axons (**B**, **I**, **P**), and merged labeling (**C**, **J**, **Q**) are shown. Striatonigral axon (green) and corticofugal axon (red) trajectories are malformed in both ventral forebrain-specific

defects within *Foxg1*^{IRES-cre}-driven mutants suggests that primarily striatal, rather than diencephalic, *Isl1* inactivation drives TCA defects. Embryonic control and *Isl1* cKO TCA (blue) and striatonigral axon (green) trajectories are summarized in Figure 6J–L.

Together, our observations in *Isl1* cKOs implicate dSPN *Isl1* expression, rather than diencephalic *Isl1* expression, in the guidance of CFAs and TCAs. Although CFAs do appear to rely, at least in part, on *Isl1* expression within the rTh to prevent CFAs destined for the brainstem and spinal cord (i.e., corticocerebral axons) from instead misrouting into the thalamus, the defasciculation and aberrant trajectories present in both permutations of *Isl1* inactivation show that telencephalic (i.e., dSPN) loss of *Isl1* is sufficient to misroute CFAs and, to a lesser extent, TCAs.

Striatonigral axon defects precede corticofugal defects in embryonic *Isl1* cKOs

If dSPN axons pioneer the internal capsule, then disruptions in their outgrowth should precede malformations of CFAs and TCAs. We tested this by tracing these axons in *Foxg1*^{IRES-cre}-driven *Isl1* cKOs at an earlier developmental time point. By E14.5, striatonigral axon outgrowth abnormalities are already visible as they extend into the SNr (Fig. 7A–D). In contrast, mutant CFAs have only reached the lateral striatum at this stage and are not yet visibly disrupted when compared with control projections at this stage (Fig. 7E–H). This suggests that CFAs are able to navigate the striatum and become misrouted at later time points after they have interacted with the misrouted dSPN axons that have already traversed the internal capsule/cerebral peduncle. Interestingly, however, TCAs have already begun exhibiting the mild ventral misrouting and defasciculation that is seen at later stages (Fig. 7I–L, arrows). By this stage, dSPN axons and TCAs have already interacted at the level of the GP; our data tracing these axons shows them associating as early as E12.5 (Fig. 1H). Disrupted mutant striatonigral axons and/or dysfunctional guidepost populations within the GP are likely driving these TCA defects.

Normal formation of the striatonigral pathway in *Fezf2* mutants

Defects in corticothalamic pathway formation can drive defects within the thalamocortical pathway and vice versa (Stoykova et al., 1996; Tuttle et al., 1999; Hevner et al., 2001; 2002; Jones et al., 2002; Chen et al., 2012). Given the reciprocal nature of TCA and CTA outgrowth, we next wanted to examine whether reciprocal interactions occur between striatonigral axons and CFAs and, in particular, to determine whether an intact

descending corticofugal pathway is required for normal striatonigral pathway formation. To address this idea, we examined *Fezf2*-null mutants for which an *EGFP-IRES-PLAP* cassette was inserted into the *Fezf2* open reading frame (Chen et al., 2005). Homozygous *Fezf2*-null mutants exhibit an absence of corticospinal projections and reductions in cortical projections to the midbrain and pons (Chen et al., 2005, 2008; McKenna et al., 2011). *Fezf2* mutants also have CTA/TCA defects (Komuta et al., 2007). Notably, the ascending TCA defects observed in *Fezf2* mutants are more severe than those seen in our *Isl1* mutants and are attributed to the established interdependence between CTAs and TCAs for appropriate pathfinding.

We crossed the *Fezf2* mutant line with *Sox8-EGFP BAC* reporter mice to examine dSPN axon outgrowth at embryonic stages. Comparing *Fezf2* mutants (*Fezf2*^{PLAP/PLAP}; *Sox8-EGFP*) with controls (*Fezf2*^{PLAP/+}; *Sox8-EGFP*) shows that the development of dSPN axons appears normal in that they are well organized, take normal trajectories around the STN (Fig. 8A,B, arrowheads), and reach the SNr (Fig. 8A,B, arrows). PLAP staining confirmed that the corticospinal tract is indeed absent in the *Fezf2* mutants; corticospinal fibers are not visible within the cerebral peduncle of mutants but are present in controls (Fig. 8C–D'). Finally, we also assessed striatal projections at P21 using DARPP-32 staining. As seen embryonically, the striatal direct pathway appears normally formed in postnatal *Fezf2* mutants (Fig. 8E,F, arrows).

These data confirm that an intact corticofugal pathway is not required for the normal formation of the striatonigral (direct) pathway. As dSPN axons precede CFAs through the forming internal capsule/cerebral peduncle, it is perhaps not surprising that defects within CFA projections do not disrupt striatonigral pathway formation. Overall, our findings in *Fezf2* mutants support the notion that dSPN axons pioneer the internal capsule/cerebral peduncle and serve a major role in guiding the descending CFAs that follow them.

Differential gene expression in the forming striatum of *Isl1* cKOs

We next wanted to determine the potential molecular mechanisms by which dSPN axons mediate the guidance of CFAs and TCAs as well as the correct formation of the internal capsule/cerebral peduncle. To identify potential candidates involved in striatal direct pathway development, we performed RNA-seq on tissue dissected from the E18.5 LGE and forming striatum of control (*Isl1*^{flx/flx}) and *Isl1* cKO (*Dlx1-cre*; *Isl1*^{flx/flx}) mice (Fig. 9A). We defined DEGs as those with a Benjamini–Hochberg-corrected false discovery rate < 0.05 and a log₂ fold change > 0.5. The majority of DEGs are downregulated in *Isl1* mutants (270 of 445, 60.7%), consistent with *Isl1* functioning as a transcriptional activator (Fig. 9A). The entire gene list (DEGs and non-DEGs) has been included as an extended data table (Extended Data Fig. 9-1).

Figure 9B shows a volcano plot of the DEGs with selected genes involved in neural development indicated. Several factors previously shown to be involved in SPN development and/or axon pathfinding are differentially regulated in our dataset, including *Ikzf1* (Agoston et al., 2007; Martín-Ibáñez et al., 2010), *Zfx3* (Zhang et al., 2019), and *Plexind1* (Chauvet et al., 2007; Ding et al., 2011; Burk et al., 2017). To identify additional DEGs involved in biological processes possibly related to dSPN axon pathfinding, we performed GO enrichment analysis through GOnet (Pomazny et al., 2018). GO terms with an adjusted *p*-

←

and telencephalon-specific *Isl1* cKOs, but only ventral forebrain-specific *Isl1* cKOs exhibit excess routing of corticofugal fibers into the thalamus (B, I, P, compare open arrowheads). High-powered images of *Sox8-EGFP/Fezf2-TdTomato* double-labeling at rostral (D, K, R; C, J, Q, solid boxes) or caudal (E, L, S; C, J, Q, dotted boxes) levels further highlight corticofugal axon disorganization, ventral deviation (D, K, R, compare arrows), and abnormal routing through the cerebral peduncle/SNr (E, L, S) in *Isl1* mutants. *Foxp2* (STN marker, boundaries outlined) double-labeling with either *Sox8-EGFP* (F, M, T) or *Fezf2-TdTomato* (G, N, U) shows that striatonigral and corticofugal axons override the STN in both ventral forebrain-specific and telencephalon-specific *Isl1* cKOs. V–X, Cartoon diagrams illustrating *Isl1* expression (yellow) and altered direct (green) and corticofugal (red) pathway axon trajectories in controls (V), ventral forebrain-specific *Isl1* cKOs (W), and telencephalon-specific *Isl1* cKOs (X). cp, Cerebral peduncle; CTX, cortex; ic, internal capsule; STM, striatum; Th, thalamus. Scale bars, 500 μm.

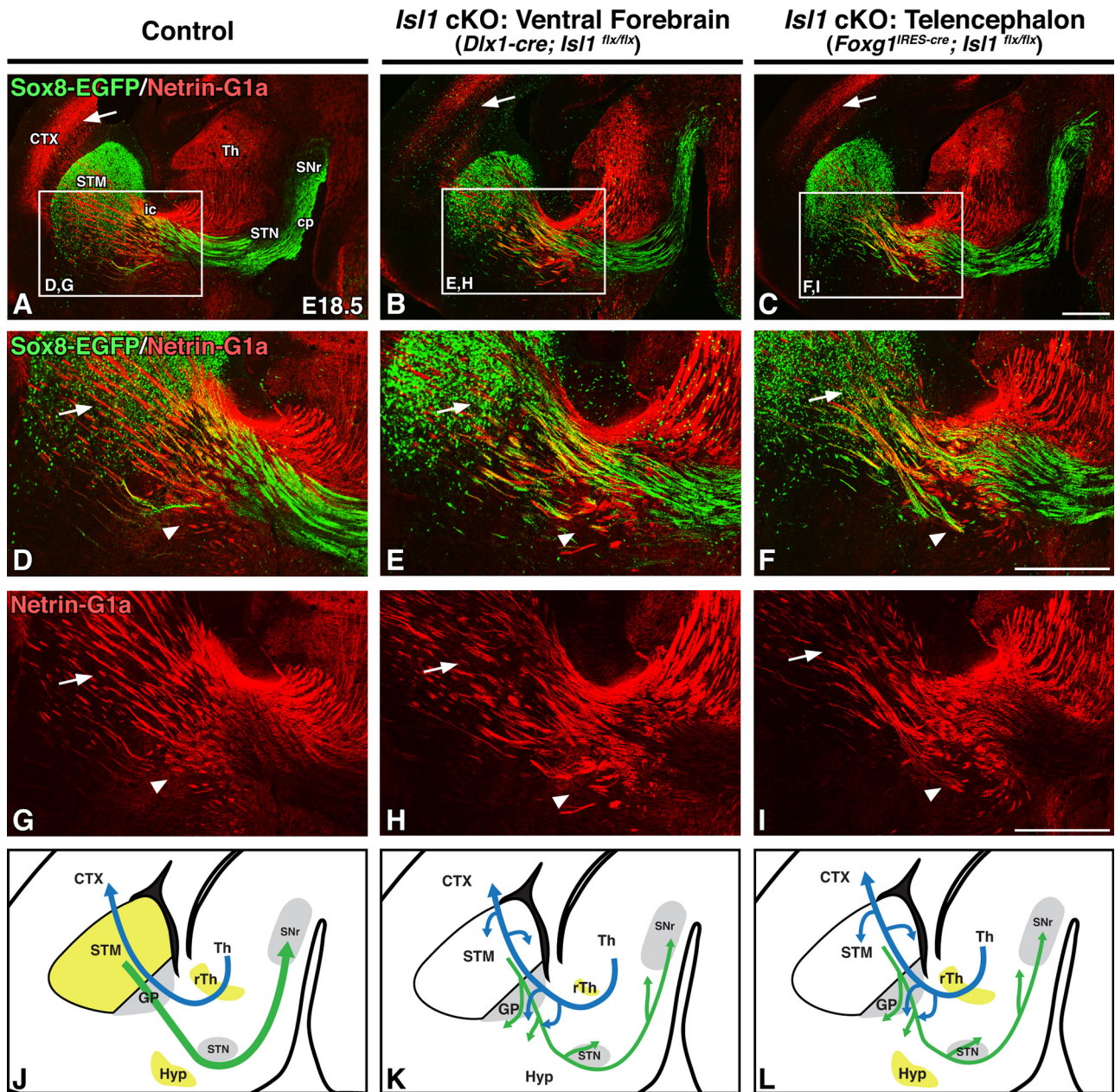


Figure 6. Striatal loss of *Isl1* results in mild thalamocortical defects at embryonic stages. **A–I**, Sagittal brain sections of E18.5 controls (*Dlx1-cre; Isl1^{flx/flx}+*; *Sox8-EGFP* or *Foxg1^{IRES-cre}; Isl1^{flx/flx}+*; *Sox8-EGFP*, $n = 6$; **A, D, G**), ventral forebrain-specific *Isl1* cKOs (*Dlx1-cre; Isl1^{flx/flx}*; *Sox8-EGFP*, $n = 3$; **B, E, H**), and telencephalon-specific *Isl1* cKOs (*Foxg1^{IRES-cre}; Isl1^{flx/flx}*; *Sox8-EGFP*, $n = 3$; **C, F, I**). *Sox8-EGFP/Netrin-G1a* double-labeling of direct pathway axons/thalamocortical axons (**A–C**) and high-power *Sox8-EGFP/Netrin-G1a* double-labeling (**D–F**; **A–C**, boxes) or *Netrin-G1a* single-labeling (**G–I**; **A–C**, boxes) is shown. Thalamocortical axons in both ventral forebrain-specific and telencephalon-specific *Isl1* cKOs reach the cortex (**A–C**, arrows) but are defasciculated (**D–F**, **G–I**, compare arrows) with ventral deviation (**D–F**, **G–I**, compare arrowheads). **J–L**, Cartoon diagrams illustrating *Isl1* expression (yellow) and altered direct pathway (green) and thalamocortical (blue) pathway axon trajectories in controls (**J**), ventral forebrain-specific *Isl1* cKOs (**K**), and telencephalon-specific *Isl1* cKOs (**L**). CTX, Cortex; ic, internal capsule; STM, striatum; Th, thalamus. Scale bars, 500 μm .

value < 0.05 were defined as significantly enriched. This analysis is provided as an extended data table (Extended Data Fig. 9–2). We focused on potential candidate factors previously implicated in neurologic disorders that were also significantly enriched for GO terms related to axon pathfinding including cell adhesion, cell–cell signaling, and cellular metabolism. We also made use of available single-cell transcriptomic data generated from embryonic mouse brain tissue (Loo et al., 2019) to further narrow our interests to genes that were determined to be expressed within dSPNs; this for the purpose of identifying possible candidate factors involved in processes mediated by dSPN axons. Selected DEGs of interest identified in this manner are shown linked to

distinct significantly enriched GO terms relevant to axon outgrowth and guidance (Fig. 9C).

Upregulated DEGs of interest include Ptprk, Cntn5, Foxp4, Zfx3, and Angpt1

Ptprk, a receptor-type protein tyrosine phosphatase, has previously been shown to play roles in mediating homophilic axonal interactions and to stimulate neurite outgrowth (Drosopoulos et al., 1999). *Cntn5* is a cell adhesion molecule implicated in ASD and has been studied for its roles in thalamocortical system wiring (Kleijer et al., 2015) and neurite outgrowth (Ogawa et al., 2001). *Foxp4*, although relatively understudied in neurologic

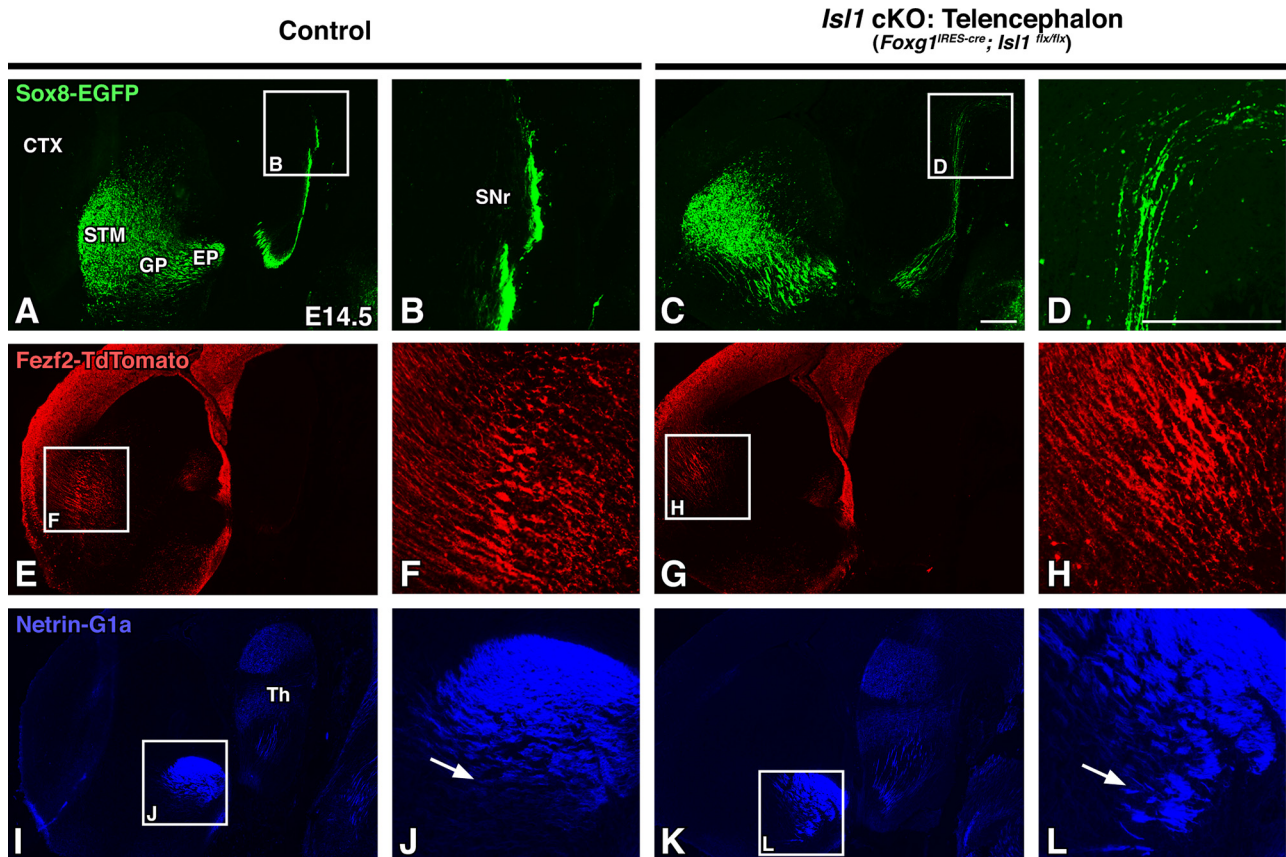


Figure 7. Striatonigral defects in *Is1* mutants appear before visible corticofugal defects. **A–L**, Sagittal brain sections of E14.5 controls (*Foxg1^{RES-cre}; Is1^{flx/+}; Sox8-EGFP; Fezf2-TdTomato* or *Is1^{flx/flx}; Sox8-EGFP; Fezf2-TdTomato*, $n = 3$; **A, B, E, F, I, J**) and *Is1* cKOs (*Foxg1^{RES-cre}; Is1^{flx/flx}; Sox8-EGFP; Fezf2-TdTomato*, $n = 3$; **C, D, G, H, K, L**) at low (**A, C, E, G, I, K**) and high (**B, D, F, H, J, L**; **A, C, E, G, I, K** boxes) power are shown. Sox8-EGFP labeling of direct pathway axons show that mutant striatonigral axons are disorganized as they project to the SNr (**A–D**). Mutant corticofugal axons appear normal at this stage as illustrated by Fezf2-TdTomato labeling (**E–H**). Netrin-G1a labeling of thalamocortical axons exhibit ventral misrouting and disorganization (**I–L**, compare **J, L**, arrows). CTX, Cortex; STM, striatum; Th, thalamus. Scale bars, 250 μm .

disease compared with its forkhead transcription factor family members *Foxp1* and *Foxp2*, has been linked to speech/language delays (Snijders Blok et al., 2021) and generalized neurodevelopmental disorder (Charng et al., 2016). *Zfhx3* is a zinc finger transcription factor necessary for the survival and differentiation of late-born dSPNs (Zhang et al., 2019). Finally, *Angpt1* is a vascular factor studied for its roles in neurogenesis (Rosa et al., 2010), neurite extension (Chen et al., 2009), and axon outgrowth (Kolar et al., 2017; Toma et al., 2020).

Downregulated DEGs of interest include Nrxn1, Serpine2, Grik2, Cadm2, Prkcd, Plxnd1, Sema3d, Col25a1, Nexn, and Ikzf1
Nrxn1, a presynaptic cell adhesion molecule linked to ASD, attention-deficit/hyperactivity disorder, schizophrenia, and intellectual disability (Al Shehhi et al., 2019), has also been studied for its role in regulating synaptic circuitry within the basal ganglia (Davatolhagh and Fuccillo, 2021). *Serpine2* is a secreted serine protease inhibitor; dysregulation of this factor leads to neuronal and motor deficits secondary to axonal dysfunction (Meins et al., 2001). *Serpine2* has also been shown to have roles in promoting neurite extension (Guenther et al., 1985; Farmer et al., 1990) and in postinjury neuron survival (Houenou et al., 1995; Smith-Swintosky et al., 1995; Donovan et al., 1997). *Grik2*, a kainate receptor subunit, is a regulator of synapse maturation (Lanore et al., 2012). Loss-of-function mutations in *Grik2* have been linked to intellectual disability, ASD, epilepsy, and dystonia (Jamain et al., 2002; Bonaglia et al., 2008; Córdoba et al., 2015).

In addition, ataxia, hypotonia, stereotyped behaviors, short attention span, and intellectual disability present in a human proband were attributed to a gain-of-function mutation in *Grik2* (Guzmán et al., 2017). *Cadm2* is a synaptic cellular adhesion molecule that mediates both homophilic and heterophilic axon–axon interactions (Fogel et al., 2007; Niederkofler et al., 2010; Frei et al., 2014). *Prkcd* is a protein receptor kinase regulating neurite induction and extension (Sakaue et al., 2003; Ling et al., 2004) as well as growth cone dynamics (Kawano et al., 1997). *Plxnd1* has been studied for its role in striatal circuit formation; mutations in *Plxnd1* or in *Sema3e*, a secreted ligand for this receptor, result in disruptions in striatonigral and thalamostriatal circuits (Chauvet et al., 2007; Ding et al., 2011; Ehrman et al., 2013; Burk et al., 2017). *Sema3e* mutants additionally exhibit striatonigral outgrowth defects (Ehrman et al., 2013); a separate class 3 semaphorin family member, *Sema3d*, is differentially regulated in our dataset. *Sema3d* binds to neuropilin receptors and is a classic axon guidance factor important for axon–axon interactions and fasciculation (Wolman et al., 2004; 2007). *Sema3d* is also associated with schizophrenia (Fujii et al., 2011). *Col25a1* is a unique, transmembrane-bound collagen; *Col25a1* mutant mice exhibit defects in axon elongation and intramuscular innervation (Tanaka et al., 2014), and null mutations in humans are a genetic cause for congenital cranial dysinnervation disorder (Shinwari et al., 2015). *Nexilin* is an actin filament binding protein with roles in oligodendrocyte cell migration (Li et al., 2018) and cell adhesion (Ohtsuka et al., 1998). Finally, *Ikzf1* is

involved in neuronal differentiation within the LGE (Agoston et al., 2007; Martín-Ibáñez et al., 2010) and was previously shown to be downregulated in the *Isl1* cKO striatum (Ehrman et al., 2013).

We selected a subset of these DEGs in our *Isl1* cKO RNA-seq dataset for validation. We used *in situ* hybridization and immunolabeling to compare mRNA/protein levels within E18.5 *Isl1* cKO (*Dlx1-cre; Isl1^{flx/flx}*) or control (*Dlx1-cre; Isl1^{flx/+}*) striata. Consistent with our RNA-seq results, *Nexn*, *Cadm2*, *Grik2*, and *Serpine2* are downregulated and *Foxp4*, *Zfhx3*, and *Cntn5* are upregulated in *Isl1* mutants when compared with controls (Fig. 9D–Q).

To better understand *Isl1* function and to determine which DEGs are directly regulated by this transcription factor, we made use of a previously published *Isl1* ChIP-exo dataset generated from mouse embryonic stem cell-differentiated motor neurons (Rhee et al., 2016). We intersected our *Isl1* cKO RNA-seq dataset with a list of *Isl1*-associated genes the authors produced by assigning *Isl1*-bound enhancers to the gene with the nearest transcriptional start site. This intersection is provided as an extended data table (Extended Data Fig. 9-3). Albeit not generated from our brain region of interest, this dataset was generated from a neuronal population that aids its intersection with our RNA-seq dataset. Indeed, many of the genes identified as being *Isl1*-associated are both expressed in dSPNs and differentially regulated in *Isl1* mutants; 112 DEGs, 37 upregulated and 75 downregulated, were identified as being *Isl1*-associated (Fig. 9R). Among them are several DEGs identified as being involved in processes related to axon pathfinding including *Ptprk*, *Cntn5*, *Foxp4*, *Zfhx3* (all upregulated), and *Nrxn1*, *Grik2*, *Cadm2*, *Plxnd1*, and *Sema3d* (all downregulated).

Finally, the transcription factor *Ebf1* is also expressed in developing dSPNs, and loss-of-function mutations in this factor result in both striatonigral axon and thalamocortical defects (Garel et al., 2002; Lobo et al., 2006, 2008; Tinterri et al., 2018). To examine whether our putative candidates are commonly dysregulated in *Ebf1* mutants, we intersected our dataset with an RNA-seq dataset generated from E17 LGE/striatum of ventral forebrain-specific *Ebf1* cKOs (Tinterri et al., 2018). We defined DEGs from the *Ebf1* cKO RNA-seq dataset using the same parameters as our *Isl1* cKO RNA-seq dataset (FDR < 0.05, log₂FC > 0.5). This intersection is provided as an extended data table (Extended Data Fig. 9-4). Our analysis revealed that *Isl1* and *Ebf1* cKOs share 53 genes that are differentially regulated from their corresponding controls; 6 upregulated in both mutants, 44 downregulated in both mutants, and 3 oppositely regulated—*Clstn2*, *Lmo4*, and *Sv2c* are downregulated in *Isl1* mutants but upregulated in *Ebf1* mutants (Fig. 9S). Many of the genes identified to be relevant to axon pathfinding are among the shared genes including *Ptprk* (upregulated), and *Col25a1*, *Nexn*, *Plxnd1*, and *Prkcd* (all downregulated). These DEGs thus warrant further investigation with respect to striatonigral axon outgrowth and internal capsule/cerebral peduncle defects common to both mutants.

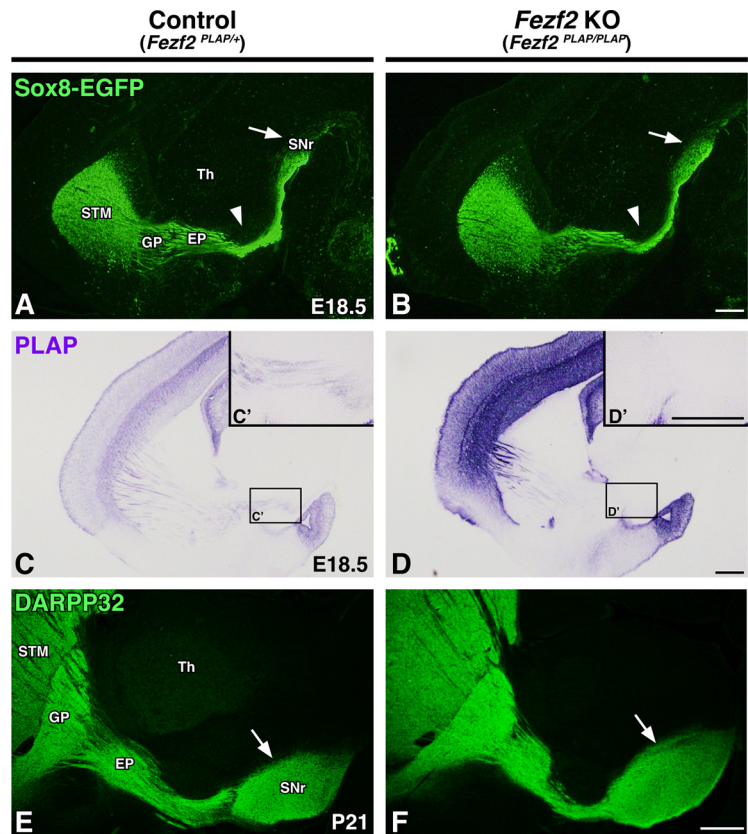


Figure 8. The corticofugal pathway is not required for proper striatonigral pathway formation. **A–D**, Sagittal brain sections of E18.5 controls (*Fezf2^{PLAP/+}*; *Sox8-EGFP*, $n = 3$; **A**, **C**) and *Fezf2*-nulls (*Fezf2^{PLAP/PLAP}*; *Sox8-EGFP*, $n = 3$; **B**, **D**) are shown. *Sox8-EGFP* labeling of direct pathway axons (**A**, **B**, arrows) shows that *Fezf2* mutants have normal direct pathway organization and innervation of the SNr (**A**, **B**, arrows). **C–D'**, PLAP staining to mark corticofugal axons (**C**, **D**) confirms the lack of corticospinal axon outgrowth within the internal capsule/cerebral peduncle (**C'**, **D'**, high-power inserts). **E**, **F**, DARPP-32 labeling of P21 control (*Fezf2^{PLAP/+}*, $n = 3$; **E**) and *Fezf2*-null (*Fezf2^{PLAP/PLAP}*, $n = 3$; **F**) sagittal sections show that striatal projections are grossly normal at postnatal stages. STM, Striatum; Th, thalamus. Scale bars, 250 μ m.

Discussion

In this study, we have identified novel contributions of basal ganglia circuitry to the proper formation of the ascending and descending tracts of the internal capsule and cerebral peduncle. We have characterized the normal spatiotemporal relationships among striatonigral axons, ascending TCAs, and descending CFAs during embryonic development. In doing so, we have shown that dSPN axons both pioneer the internal capsule/cerebral peduncle and form close associations with TCAs and CFAs at several points along their respective trajectories through the ventral telencephalon, diencephalon, and midbrain, thus implicating dSPN axons in the guidance of these forebrain trajectories. Supporting this notion, we have used *Isl1* cKOs as a model of impaired striatonigral axon outgrowth to demonstrate that disruption of striatal circuitry impacts internal capsule formation in a non-cell autonomous manner. Moreover, we have made use of region-specific drivers of Cre-mediated recombination to show that these malformations are not because of the loss of *Isl1* expression within diencephalic populations bordering the internal capsule/cerebral peduncle, but rather are from *Isl1* inactivation within LGE-derived populations.

Our spatiotemporal analysis showed that the principal point at which dSPN axons, TCAs, and CFAs all interact occurs at the level of the GP. The MGE and MGE-derived GP are recognized as intermediate targets for forming TCAs and CFAs (Métin and

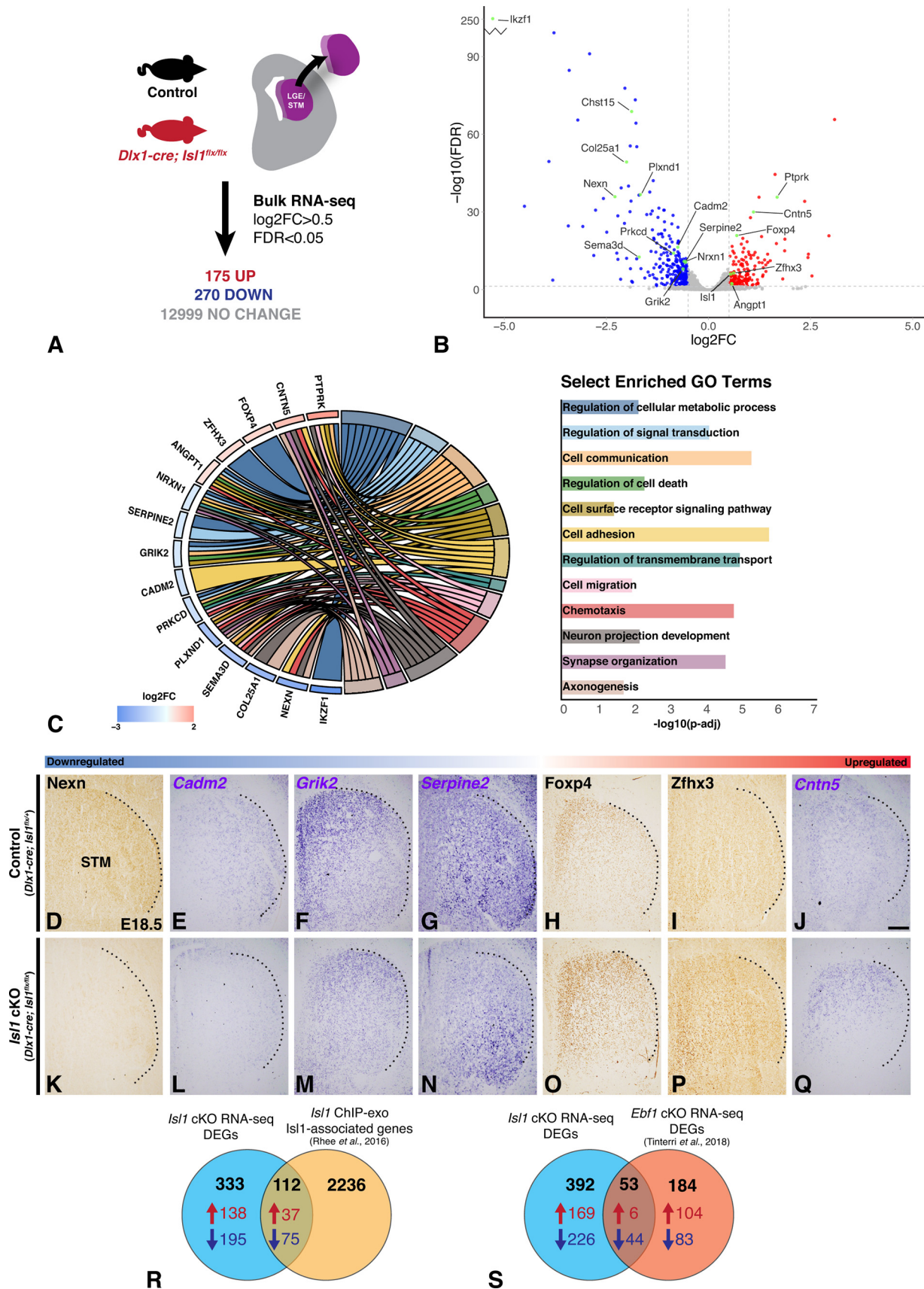


Figure 9. Transcriptomic analysis of *Isl1* cKOs identifies candidate genes with known roles in metabolism, cell–cell adhesion, growth cone dynamics, and extracellular matrix composition. **A**, Summary of RNA-seq experiment performed on dissected LGE/striatum from E18.5 control (*Isl1^{flox/flox}*, *n* = 4) and *Isl1* cKO (*Dlx1-cre; Isl1^{flox/flox}*, *n* = 4) mouse brains. The complete gene list including DEGs and non-DEGs is provided in Extended Data Figure 9-1. **B**, Volcano plot illustrating global gene expression changes in *Isl1* cKOs with notable genes highlighted. **C**, Chord diagram of select DEGs (ordered by log₂FC) identified in *Isl1* cKOs linked to select significantly enriched GO terms (adjusted *p*-value < 0.05). The complete dataset from this GO term analysis is provided in

Godement, 1996; Marín et al., 2002) and contain several guidepost populations that contribute to their trajectories (López-Bendito et al., 2006; Bielle et al., 2011b; Kaur et al., 2020). Our observations in *Isl1* cKOs suggest that TCAs and CFAs rely not only on these cellular guidepost populations, but also on striatonigral projections for their correct trajectories. Indeed, we are not the first to raise this notion; both MGE guidepost populations and striatal axons themselves are implicated in the TCA/CTA malformations observed in *Pcdh10* mutants, a gene coding for a protocadherin (OL-protocadherin) localized on striatal axons (Uemura et al., 2007). Our data corroborate these findings and additionally suggest a novel, direct role for striatonigral fibers in guiding corticosubcerebral axons after they diverge from CTAs caudal to the GP.

Among the guidepost populations located within the GP is the group of LGE-derived corridor cells that form a permissive region for the extension of TCAs through an otherwise nonpermissive MGE (López-Bendito et al., 2006; Bielle et al., 2011b). As these cells express *Isl1*, among other SPN markers, they are impacted by both the *Dlx1*- and *Foxg1*-cre drivers we used to regionally inactivate *Isl1*. Although we have shown that corridor cells are appropriately localized in *Isl1* cKOs, we cannot completely dissociate the impact of dysfunctional corridor cells on internal capsule formation from that of malformed striatonigral axons. Indeed, the embryonic TCA malformations present in *Isl1* mutants do support a role for corridor cell dysfunction; mutant TCAs are ventrally deviated with reduced fibers traversing the striatum, suggesting that their ability to ascend through the corridor may be impeded.

Although malformations of *Isl1* mutant TCAs likely arise from multiple disrupted populations, our findings strongly support a direct role for striatonigral axons in the observed abnormal trajectories of mutant CFAs descending within the internal capsule/cerebral peduncle. The disrupted CFA topography is striking; *Isl1* mutant CFAs misroute in almost identical ways to the malformed dSPNs that pioneer this region. In control animals, these pathways course alongside one another, but as two distinct axon bundles with highly stereotyped trajectories; CFAs remain dorsal to dSPN axons through the internal capsule before crossing ventral to them at the STN to form the cerebral peduncle. Heterotypic and homotypic transaxonal interactions, both attractive and repulsive, establish and maintain the balance in axonal adhesion required for the proper fasciculation and sorting of pioneer–follower axons (for review, see Spעד and Poulain, 2020). Attractive interactions keep discrete tracts

coursing together while repulsive interactions allow for these same tracts to form distinct bundles that can selectively defasciculate and diverge toward different targets. The defects between *Isl1* mutant dSPN axon/CFA trajectories suggest that the balance between heterotypic and/or homotypic signaling mediating this pioneer–follower relationship is disrupted within mutant dSPNs.

By what mechanisms do striatonigral projections navigate the internal capsule/cerebral peduncle and guide CFAs? Genes involved in processes related to axon pathfinding, such as cell adhesion (e.g., *Cadm2*, *Cntn5*), growth cone dynamics (e.g., *Prkcd*), and synapse formation (e.g., *Grik2*, *Nrxn1*) are altered in *Isl1* mutants, suggesting specific molecular mechanisms by which dSPN axons might mediate this role. Notable among these DEGs is *Plxnd1*, which has previously been shown to be downregulated in *Isl1* mutants (Lu et al., 2014) and a proposed direct target of *Isl1* in motor neurons (Rhee et al., 2016). Striatonigral projections take widened trajectories in *Plxnd1*-null mice (Burk et al., 2017) and also in null mice for *Sema3e*, the gene encoding a *Plxnd1*-repulsive ligand (Ehrman et al., 2013). Both phenotypes are reminiscent of our observed *Isl1* mutant dSPN axons; however, CFA defects have not been described for either mutant.

It should be noted that factors involved in striatonigral axon guidance of CFAs need not necessarily be dysregulated in our dataset. If factors driving dSPN axon outgrowth are disrupted, the mere absence of those axons reaching the appropriate places at the appropriate times, despite retaining signaling/guidance capabilities and normal expression of factors involved in guiding CFAs, might still cause CFA misrouting. This possibility is supported, at least in part, by our anatomic analyses in *Isl1* cKOs as misrouted CFA fibers follow the aberrant paths already laid down by mutant striatonigral axons; the axon–axon interactions used by dSPN axons to direct the pathfinding of descending CFAs may thus still be intact. On the other hand, the stereotyped fasciculation of these two axon pathways into discrete bundles is not present, suggesting that other molecular mechanisms, likely to be present in our intersected transcriptomic datasets, are indeed disrupted. *Isl1* and *Ebf1* mutants (Tinterri et al., 2018) have distinct, but overlapping striatonigral axon outgrowth defects. Comparing these datasets allows us to separate DEGs mediating disrupted processes common to these mutants from those that drive abnormalities unique to each (e.g., early dSPN cell death in *Isl1* mutants vs disruption of patch/matrix architecture in *Ebf1* mutants).

Reciprocal cues from CFAs might also regulate dSPN pathway outgrowth, elaboration, and/or maintenance. However, given that dSPNs precede CFA entry into the internal capsule, we predicted that disruption in CFA outgrowth would not impact dSPN axon trajectories. This idea is supported by our findings in *Fefz2* mutants, which exhibit a grossly normal striatonigral pathway, even into postnatal stages, despite the near absence of CFAs reaching the midbrain. Thus, in contrast to CTAs and TCAs whose trajectories are interdependent (Stoykova et al., 1996; Tuttle et al., 1999; Hevner et al., 2001, 2002; Jones et al., 2002; Chen et al., 2012), there is a nonreciprocal requirement for dSPNs in the formation of CFA trajectories. We did not explore the impact of TCA malformation, such as that seen in *Gbx2* mutants (Miyashita-Lin et al., 1999; Hevner et al., 2002; Chatterjee et al., 2012), on striatonigral pathway integrity. However, given the limited associations between TCAs and the majority of dSPN axons beyond the GP, a role for TCAs seems unlikely.

Our findings implicate striatal malformations in defective neural circuit assembly within the internal capsule/cerebral

←

Extended Data Figure 9-2. **D–Q**, Immunohistochemistry (**D, H, I, K, O, P**) or *in situ* hybridization (**E, F, G, J, L, M, N, Q**) validating DEGs in E18.5 control (*Dlx1*-cre; *Isl1*^{flx/+}, $n \geq 3$; **D–J**) and *Isl1* cKO (*Dlx1*-cre; *Isl1*^{flx/flx}, $n \geq 3$; **K–Q**) coronal brain sections. Candidate factors are ordered by log₂FC. Dashed lines indicate the lateral border of the STM. *Nexn* (**D, K**), *Cadm2* (**E, L**), *Grik2* (**F, M**), and *Serpine2* (**G, N**) are downregulated, and *Foxp4* (**H, O**), *Zfhx3* (**I, P**), and *Cntn5* (**J, Q**) are upregulated in *Isl1* cKOs. **R**, Venn diagram summarizing the intersection of *Isl1* cKO DEGs with *Isl1*-associated genes from a previously published *Isl1* ChIP-exo dataset (Rhee et al., 2016) generated from mouse embryonic stem cell differentiated motor neurons. Additional data from this intersection are provided in Extended Data Figure 9-3. **S**, Venn diagram summarizing intersection of *Isl1* cKO DEGs with DEGs identified from an *Ebf1* cKO RNA-seq dataset (Tinterri et al., 2018) generated from E17.5 control (*Dlx5/6*-cre; *Ebf1*^{flx/+}) and *Ebf1* cKO (*Dlx5/6*-cre; *Ebf1*^{flx/-}) striatal tissue. Additional data from this intersection are provided in Extended Data Figure 9-4. STM, Striatum. DEGs for RNA-seq datasets defined by log₂FC > 0.5 and FDR < 0.05. Parameters used for the generation of ChIP-exo *Isl1*-associated gene list are defined in the original publication (Rhee et al., 2016). Scale bar, 200 μ m.

peduncle, broadening the potential impact that primary basal ganglia insults can have on neural circuit assembly and function. In fact, we previously found that *Isl1* cKOs are hyperlocomotive and blunted in response to stimulants (Ehrman et al., 2013). The current findings demonstrate a significant secondary effect on CFAs, and in particular corticosubcerebral axons, in *Isl1* cKOs. This complicates our interpretation of the behavioral findings since *Fezf2* mutants, which have severe CFA defects, also exhibit hyperlocomotion (Hirata et al., 2004). In humans, developmental defects originating within the basal ganglia have rarely been described; however, two recently identified homozygous variants in the homeobox transcription factor *GSX2* have been reported in unrelated human patients both presenting with not only basal ganglia dysgenesis, but also corticospinal tract abnormalities (De Mori et al., 2019). In mice, *Gsx2* is required for proper striatal development (for review, see Rubenstein and Campbell, 2020) and together with *Gsx1* is necessary for correct CFA/TCA development (Yun et al., 2003). Both human *GSX2* variants result in nearly complete loss of the putamen and altered formation of the caudate nucleus (De Mori et al., 2019), which is certain to impact both iSPNs and dSPNs. Accordingly, CFAs appear to be misrouted dorsal to the pons in both patients, similar to what we observe in *Isl1* cKOs. Thus, prenatal basal ganglia insults, due either to genetic variation or lesion (e.g., stroke), may have broad behavioral implications for voluntary movements, cognition, and emotion in humans.

To conclude, we have identified a nonreciprocal requirement for dSPNs in the guidance of CFAs through the internal capsule and cerebral peduncle. Our data add to previous work in a variety of genetic mouse mutants with striatal circuit disruptions that also exhibit TCA/CTA defects. Future work will focus on examining the mechanisms by which pioneer dSPN axon growth cones are themselves guided to the SNr and on interrogating the axon-axon signals used to guide CFAs.

References

- Agoston DV, Szemes M, Dobi A, Palkovits M, Georgopoulos K, Gyorgy A, Ring MA (2007) Ikaros is expressed in developing striatal neurons and involved in enkephalinergic differentiation. *J Neurochem* 102:1805–1816.
- Al Shehhi M, Forman EB, Fitzgerald JE, McInerney V, Krawczyk J, Shen S, Betts DR, Ardle LM, Gorman KM, King MD, Green A, Gallagher L, Lynch SA (2019) NRXN1 deletion syndrome; phenotypic and penetrance data from 34 families. *Eur J Med Genet* 62:204–209.
- Anderson KD, Reiner A (1991) Immunohistochemical localization of DARPP-32 in striatal projection neurons and striatal interneurons: implications for the localization of D1-like dopamine receptors on different types of striatal neurons. *Brain Res* 568:235–243.
- Auladell C, Pérez-Sust P, Supèr H, Soriano E (2000) The early development of thalamocortical and corticothalamic projections in the mouse. *Anat Embryol (Berl)* 201:169–179.
- Báez-Mendoza R, Schultz W (2013) The role of the striatum in social behavior. *Front Neurosci* 7:233.
- Bielle F, Marcos-Mondejar P, Keita M, Mailhes C, Verney C, Nguyen Bacharvet K, Tessier-Lavigne M, Lopez-Bendito G, Garel S (2011a) Slit2 activity in the migration of guidepost neurons shapes thalamic projections during development and evolution. *Neuron* 69:1085–1098.
- Bielle F, Marcos-Mondejar P, Leyva-Díaz E, Lokmane L, Mire E, Mailhes C, Keita M, García N, Tessier-Lavigne M, Garel S, López-Bendito G (2011b) Emergent growth cone responses to combinations of Slit1 and Netrin 1 in thalamocortical axon topography. *Curr Biol* 21:1748–1755.
- Bonaglia MC, Ciccone R, Gimelli G, Gimelli S, Marelli S, Verheij J, Giorda R, Grasso R, Borgatti R, Pagone F, Rodríguez L, Martínez-Frías ML, van Ravenswaaij C, Zuffardi O (2008) Detailed phenotype-genotype study in five patients with chromosome 6q16 deletion: narrowing the critical region for Prader-Willi-like phenotype. *Eur J Hum Genet* 16:1443–1449.
- Burk K, Mire E, Bellon A, Hocine M, Guillot J, Moraes F, Yoshida Y, Simons M, Chauvet S, Mann F (2017) Post-endocytic sorting of Plexin-D1 controls signal transduction and development of axonal and vascular circuits. *Nat Commun* 8:14508.
- Cai CL, Liang X, Shi Y, Chu PH, Pfaff SL, Chen J, Evans S (2003) *Isl1* identifies a cardiac progenitor population that proliferates prior to differentiation and contributes a majority of cells to the heart. *Dev Cell* 5:877–889.
- Chapman H, Riesenberger A, Ehrman LA, Kohli V, Nardini D, Nakafuku M, Campbell K, Waclaw RR (2018) *Gsx* transcription factors control neuronal versus glial specification in ventricular zone progenitors of the mouse lateral ganglionic eminence. *Dev Biol* 442:115–126.
- Chang W-L, et al. (2016) Exome sequencing in mostly consanguineous Arab families with neurologic disease provides a high potential molecular diagnosis rate. *BMC Med Genomics* 9:42.
- Chatterjee M, Li K, Chen L, Maisano X, Guo Q, Gan L, Li JY (2012) *Gbx2* regulates thalamocortical axon guidance by modifying the LIM and Robo codes. *Development* 139:4633–4643.
- Chauvet S, Cohen S, Yoshida Y, Fekrane L, Livet J, Gayet O, Segu L, Buhot MC, Jessell TM, Henderson CE, Mann F (2007) Gating of *Sema3E/PlexinD1* signaling by neuropilin-1 switches axonal repulsion to attraction during brain development. *Neuron* 56:807–822.
- Chen B, Schaevitz LR, McConnell SK (2005) *Fezl* regulates the differentiation and axon targeting of layer 5 subcortical projection neurons in cerebral cortex. *Proc Natl Acad Sci U S A* 102:17184–17189.
- Chen B, Wang SS, Hattox AM, Rayburn H, Nelson SB, McConnell SK (2008) The *Fezf2-Ctip2* genetic pathway regulates the fate choice of subcortical projection neurons in the developing cerebral cortex. *Proc Natl Acad Sci U S A* 105:11382–11387.
- Chen X, Fu W, Tung CE, Ward NL (2009) Angiopoietin-1 induces neurite outgrowth of PC12 cells in a Tie2-independent, beta1-integrin-dependent manner. *Neurosci Res* 64:348–354.
- Chen Y, Magnani D, Theil T, Pratt T, Price DJ (2012) Evidence that descending cortical axons are essential for thalamocortical axons to cross the pallial-subpallial boundary in the embryonic forebrain. *PLoS One* 7:e33105.
- Córdoba M, Rodríguez S, González Morón D, Medina N, Kauffman MA (2015) Expanding the spectrum of *Grik2* mutations: intellectual disability, behavioural disorder, epilepsy and dystonia. *Clin Genet* 87:293–295.
- Davatulhagh MF, Fuccillo MV (2021) *Neurexin1α* differentially regulates synaptic efficacy within striatal circuits. *Cell Rep* 34:108773.
- De Carlos JA, O’Leary DD (1992) Growth and targeting of subplate axons and establishment of major cortical pathways. *J Neurosci* 12:1194–1211.
- Deck M, Lokmane L, Chauvet S, Mailhes C, Keita M, Niquille M, Yoshida M, Yoshida Y, Lebrand C, Mann F, Grove EA, Garel S (2013) Pathfinding of corticothalamic axons relies on a rendezvous with thalamic projections. *Neuron* 77:472–484.
- De Mori R, et al. (2019) Agenesis of the putamen and globus pallidus caused by recessive mutations in the homeobox gene *GSX2*. *Brain* 142:2965–2978.
- Ding JB, Oh WJ, Sabatini BL, Gu C (2011) Semaphorin 3E-Plexin-D1 signaling controls pathway-specific synapse formation in the striatum. *Nat Neurosci* 15:215–223.
- Dobin A, Davis CA, Schlesinger F, Drenkow J, Zaleski C, Jha S, Batut P, Chaisson M, Gingeras TR (2013) STAR: ultrafast universal RNA-seq aligner. *Bioinformatics* 29:15–21.
- Donovan FM, Pike CJ, Cotman CW, Cunningham DD (1997) Thrombin induces apoptosis in cultured neurons and astrocytes via a pathway requiring tyrosine kinase and RhoA activities. *J Neurosci* 17:5316–5326.
- Drosopoulos NE, Walsh FS, Doherty P (1999) A soluble version of the receptor-like protein tyrosine phosphatase kappa stimulates neurite outgrowth via a Grb2/MEK1-dependent signaling cascade. *Mol Cell Neurosci* 13:441–449.
- Edgar R, Domrachev M, Lash AE (2002) Gene Expression Omnibus: NCBI gene expression and hybridization array data repository. *Nucleic Acids Res* 30:207–210.

- Ehrman LA, Mu X, Waclaw RR, Yoshida Y, Vorhees CV, Klein WH, Campbell K (2013) The LIM homeobox gene *Isl1* is required for the correct development of the striatonigral pathway in the mouse. *Proc Natl Acad Sci U S A* 110:E4026–35.
- Farmer L, Sommer J, Monard D (1990) Glia-derived nexin potentiates neurite extension in hippocampal pyramidal cells in vitro. *Dev Neurosci* 12:73–80.
- Feng J, Xian Q, Guan T, Hu J, Wang M, Huang Y, So KF, Evans SM, Chai G, Goffinet AM, Qu Y, Zhou L (2016) *Celsr3* and *Fzd3* organize a pioneer neuron scaffold to steer growing thalamocortical axons. *Cereb Cortex* 26:3323–3334.
- Fogel AI, Akins MR, Krupp AJ, Stagi M, Stein V, Biederer T (2007) SynCAMs organize synapses through heterophilic adhesion. *J Neurosci* 27:12516–12530.
- Frei JA, Andermatt I, Gesemann M, Stoekli ET (2014) The SynCAM synaptic cell adhesion molecules are involved in sensory axon pathfinding by regulating axon-axon contacts. *J Cell Sci* 127:5288–5302.
- Fujii T, Uchiyama H, Yamamoto N, Hori H, Tatsumi M, Ishikawa M, Arima K, Higuchi T, Kunugi H (2011) Possible association of the semaphorin 3D gene (*SEMA3D*) with schizophrenia. *J Psychiatr Res* 45:47–53.
- Garel S, Yun K, Grosschedl R, Rubenstein JL (2002) The early topography of thalamocortical projections is shifted in *Ebf1* and *Dlx1/2* mutant mice. *Development* 129:5621–5634.
- Gerfen CR, Surmeier DJ (2011) Modulation of striatal projection systems by dopamine. *Annu Rev Neurosci* 34:441–466.
- Gerfen CR, Paletzki R, Heintz N (2013) GENSAT BAC cre-recombinase driver lines to study the functional organization of cerebral cortical and basal ganglia circuits. *Neuron* 80:1368–1383.
- Goedhart J, Luijsterburg MS (2020) VolcanoR is a web app for creating, exploring, labeling and sharing volcano plots. *Sci Rep* 10:20560.
- Gong S, Zheng C, Doughty ML, Losos K, Didkovsky N, Schambra UB, Nowak NJ, Joyner A, Leblanc G, Hatten ME, Heintz N (2003) A gene expression atlas of the central nervous system based on bacterial artificial chromosomes. *Nature* 425:917–925.
- Gong S, Doughty M, Harbaugh CR, Cummins A, Hatten ME, Heintz N, Gerfen CR (2007) Targeting Cre recombinase to specific neuron populations with bacterial artificial chromosome constructs. *J Neurosci* 27:9817–9823.
- Guenther J, Nick H, Monard D (1985) A glia-derived neurite-promoting factor with protease inhibitory activity. *EMBO J* 4:1963–1966.
- Guzmán YF, Ramsey K, Stolz JR, Craig DW, Huentelman MJ, Narayanan V, Swanson GT (2017) A gain-of-function mutation in the *GRIK2* gene causes neurodevelopmental deficits. *Neurol Genet* 3:e129.
- Hevner RF, Shi L, Justice N, Hsueh Y, Sheng M, Smiga S, Bulfone A, Goffinet AM, Campagnoni AT, Rubenstein JL (2001) *Tbr1* regulates differentiation of the preplate and layer 6. *Neuron* 29:353–366.
- Hevner RF, Miyashita-Lin E, Rubenstein JL (2002) Cortical and thalamic axon pathfinding defects in *Tbr1*, *Gbx2*, and *Pax6* mutant mice: evidence that cortical and thalamic axons interact and guide each other. *J Comp Neurol* 447:8–17.
- Hirata T, Suda Y, Nakao K, Narimatsu M, Hirano T, Hibi M (2004) Zinc finger gene *fez*-like functions in the formation of subplate neurons and thalamocortical axons. *Dev Dyn* 230:546–556.
- Houenou LJ, Turner PL, Li L, Oppenheim RW, Festoff BW (1995) A serine protease inhibitor, protease nexin I, rescues motoneurons from naturally occurring and axotomy-induced cell death. *Proc Natl Acad Sci U S A* 92:895–899.
- Hua R, Yu S, Liu M, Li H (2018) A PCR-based method for RNA probes and applications in neuroscience. *Front Neurosci* 12:266.
- Jamain S, Betancur C, Quach H, Philippe A, Fellous M, Giros B, Gillberg C, Leboyer M, Bourgeron T (2002) Paris Autism Research International Sibpair (PARIS) Study. Linkage and association of the glutamate receptor 6 gene with autism. *Mol Psychiatry* 7:302–310.
- Jones L, López-Bendito G, Gruss P, Stoykova A, Molnár Z (2002) *Pax6* is required for the normal development of the forebrain axonal connections. *Development* 129:5041–5052.
- Kaur N, et al. (2020) Neural stem cells direct axon guidance via their radial fiber scaffold. *Neuron* 107:1197–1211.e9.
- Kawaguchi D, Sahara S, Zembrzycki A, O'Leary DDM (2016) Generation and analysis of an improved *Foxg1*-IRES-Cre driver mouse line. *Dev Biol* 412:139–147.
- Kawano S, Okajima S, Mizoguchi A, Tamai K, Hirasawa Y, Ide C (1997) Immunocytochemical distribution of Ca^{2+} -independent protein kinase C subtypes (δ , ϵ , and ζ) in regenerating axonal growth cones of rat peripheral nerve. *Neuroscience* 81:263–273.
- Kleijer KT, Zuko A, Shimoda Y, Watanabe K, Burbach JP (2015) Contactin-5 expression during development and wiring of the thalamocortical system. *Neuroscience* 310:106–113.
- Kolar MK, Itte VN, Kingham PJ, Novikov LN, Wiberg M, Kelk P (2017) The neurotrophic effects of different human dental mesenchymal stem cells. *Sci Rep* 7:12605.
- Komuta Y, Hibi M, Arai T, Nakamura S, Kawano H (2007) Defects in reciprocal projections between the thalamus and cerebral cortex in the early development of *Fezl*-deficient mice. *J Comp Neurol* 503:454–465.
- Langen M, Schnack HG, Nederveen H, Bos D, Lahuis BE, de Jonge MV, van Engeland H, Durston S (2009) Changes in the developmental trajectories of striatum in autism. *Biol Psychiatry* 66:327–333.
- Lanore F, Labrousse VF, Szabo Z, Normand E, Blanchet C, Mulle C (2012) Deficits in morphofunctional maturation of hippocampal mossy fiber synapses in a mouse model of intellectual disability. *J Neurosci* 32:17882–17893.
- Lein ES, et al. (2007) Genome-wide atlas of gene expression in the adult mouse brain. *Nature* 445:168–176.
- Leisman G, Braun-Benjamin O, Melillo R (2014) Cognitive-motor interactions of the basal ganglia in development. *Front Syst Neurosci* 8:16.
- Li Q, Zhao H, Pan P, Ru X, Zuo S, Qu J, Liao B, Chen Y, Ruan H, Feng H (2018) *Nexilin* regulates oligodendrocyte progenitor cell migration and myelination and is negatively regulated by protease-activated receptor 1/Ras-Proximate-1 signaling following subarachnoid hemorrhage. *Front Neurol* 9:282.
- Liao Y, Smyth GK, Shi W (2014) featureCounts: an efficient general purpose program for assigning sequence reads to genomic features. *Bioinformatics* 30:923–930.
- Ling M, Tröllér U, Zeidman R, Lundberg C, Larsson C (2004) Induction of neurites by the regulatory domains of PKC δ and ϵ is counteracted by PKC catalytic activity and by the RhoA pathway. *Exp Cell Res* 292:135–150.
- Lobo MK, Karsten SL, Gray M, Geschwind DH, Yang XW (2006) FACS-array profiling of striatal projection neuron subtypes in juvenile and adult mouse brains. *Nat Neurosci* 9:443–452.
- Lobo MK, Yeh C, Yang XW (2008) Pivotal role of early B-cell factor 1 in development of striatonigral medium spiny neurons in the matrix compartment. *J Neurosci Res* 86:2134–2146.
- Lokmane L, Proviville R, Narboux-Nême N, Györy I, Keita M, Mailhes C, Léna C, Gaspar P, Grosschedl R, Garel S (2013) Sensory map transfer to the neocortex relies on pretarget ordering of thalamic axons. *Curr Biol* 23:810–816.
- Loo L, Simon JM, Xing L, McCoy ES, Niehaus JK, Guo J, Anton ES, Zylka MJ (2019) Single-cell transcriptomic analysis of mouse neocortical development. *Nat Commun* 10:134.
- López-Bendito G, Cautinat A, Sánchez JA, Bielle F, Flames N, Garratt AN, Talmage DA, Role LW, Charnay P, Marín O, Garel S (2006) Tangential neuronal migration controls axon guidance: a role for neuregulin-1 in thalamocortical axon navigation. *Cell* 125:127–142.
- Lu KM, Evans SM, Hirano S, Liu FC (2014) Dual role for *Islet-1* in promoting striatonigral and repressing striatopallidal genetic programs to specify striatonigral cell identity. *Proc Natl Acad Sci U S A* 111:E168–E177.
- Macpherson T, Morita M, Hikida T (2014) Striatal direct and indirect pathways control decision-making behavior. *Front Psychol* 5:1301.
- Marín O, Baker J, Puelles L, Rubenstein JL (2002) Patterning of the basal telencephalon and hypothalamus is essential for guidance of cortical projections. *Development* 129:761–773.
- Martín-Ibáñez R, Crespo E, Urbán N, Sergent-Tanguy S, Herranz C, Jaumot M, Valiente M, Long JE, Pineda JR, Andreu C, Rubenstein JL, Marín O, Georgopoulos K, Mengod G, Fariñas J, Bachs O, Alberch J, Canals JM (2010) *Ikaros-1* couples cell cycle arrest of late striatal precursors with neurogenesis of enkephalinergic neurons. *J Comp Neurol* 518:329–351.
- McKenna WL, Betancourt J, Larkin KA, Abrams B, Guo C, Rubenstein JL, Chen B (2011) *Tbr1* and *Fez2* regulate alternate corticofugal neuronal identities during neocortical development. *J Neurosci* 31:549–564.

- Meins M, Piosik P, Schaeren-Wiemers N, Franzoni S, Troncoso E, Kiss JZ, Brösamle C, Schwab ME, Molnár Z, Monard D (2001) Progressive neuronal and motor dysfunction in mice overexpressing the serine protease inhibitor protease nexin-1 in postmitotic neurons. *J Neurosci* 21:8830–8841.
- Merchan-Sala P, Nardini D, Waclaw RR, Campbell K (2017) Selective neuronal expression of the SoxE factor, Sox8, in direct pathway striatal projection neurons of the developing mouse brain. *J Comp Neurol* 525:2805–2819.
- Métin C, Godeмент P (1996) The ganglionic eminence may be an intermediate target for corticofugal and thalamocortical axons. *J Neurosci* 16:3219–3235.
- Miyashita-Lin EM, Hevner R, Wassarman KM, Martinez S, Rubenstein JL (1999) Early neocortical regionalization in the absence of thalamic innervation. *Science* 285:906–909.
- Molyneux BJ, Arlotta P, Hirata T, Hibi M, Macklis JD (2005) Fezl is required for the birth and specification of corticospinal motor neurons. *Neuron* 47:817–831.
- Molyneux BJ, Arlotta P, Menezes JR, Macklis JD (2007) Neuronal subtype specification in the cerebral cortex. *Nat Rev Neurosci* 8:427–437.
- Mu X, Fu X, Beremand PD, Thomas TL, Klein WH (2008) Gene regulation logic in retinal ganglion cell development: *Isl1* defines a critical branch distinct from but overlapping with *Pou4f2*. *Proc Natl Acad Sci U S A* 105:6942–6947.
- Muraleedharan R, Nardini D, Waclaw RR, Dasgupta B (2021) Analysis of reactive astrogliosis in mouse brain using in situ hybridization combined with immunohistochemistry. *STAR Protoc* 2:100375.
- Nakashiba T, Ikeda T, Nishimura S, Tashiro K, Honjo T, Culotti JG, Itohara S (2000) Netrin-G1: a novel glycosyl phosphatidylinositol-linked mammalian netrin that is functionally divergent from classical netrins. *J Neurosci* 20:6540–6550.
- Nasif S, de Souza FS, González LE, Yamashita M, Orquera DP, Low MJ, Rubinstein M (2015) *Isl1* specifies the identity of hypothalamic melanocortin neurons and is critical for normal food intake and adiposity in adulthood. *Proc Natl Acad Sci U S A* 112:E1861–E1870.
- Niederkofler V, Baeriswyl T, Ott R, Stoeckli ET (2010) Nectin-like molecules/SynCAMs are required for post-crossing commissural axon guidance. *Development* 137:427–435.
- Norman LJ, Carlisi C, Lukito S, Hart H, Mataix-Cols D, Radua J, Rubia K (2016) Structural and functional brain abnormalities in attention-deficit/hyperactivity disorder and obsessive-compulsive disorder: a comparative meta-analysis. *JAMA Psychiatry* 73:815–825.
- Obeso JA, Rodríguez-Oroz MC, Rodríguez M, Arbizu J, Giménez-Amaya JM (2002) The basal ganglia and disorders of movement: pathophysiological mechanisms. *News Physiol Sci* 17:51–55.
- Ogawa J, Lee S, Itoh K, Nagata S, Machida T, Takeda Y, Watanabe K (2001) Neural recognition molecule NB-2 of the contactin/F3 subgroup in rat: specificity in neurite outgrowth-promoting activity and restricted expression in the brain regions. *J Neurosci Res* 65:100–110.
- Ohtsuka T, Nakanishi H, Ikeda W, Satoh A, Momose Y, Nishioka H, Takai Y (1998) Nexilin: a novel actin filament-binding protein localized at cell-matrix adherens junction. *J Cell Biol* 143:1227–1238.
- Pennartz CM, Ito R, Verschuer PF, Battaglia FP, Robbins TW (2011) The hippocampal-striatal axis in learning, prediction and goal-directed behavior. *Trends Neurosci* 34:548–559.
- Pfaff SL, Mendelsohn M, Stewart CL, Edlund T, Jessell TM (1996) Requirement for LIM homeobox gene *Isl1* in motor neuron generation reveals a motor neuron-dependent step in interneuron differentiation. *Cell* 84:309–320.
- Pomaznoy M, Ha B, Peters B (2018) GONet: a tool for interactive gene ontology analysis. *BMC Bioinformatics* 19:470.
- Rapp SJ, Dershem V, Zhang X, Schutte SC, Chariker ME (2020) Varying negative pressure wound therapy acute effects on human split-thickness autografts. *J Burn Care Res* 41:104–112.
- Rhee HS, Closser M, Guo Y, Bashkurova EV, Tan GC, Gifford DK, Wichterle H (2016) Expression of terminal effector genes in mammalian neurons is maintained by a dynamic relay of transient enhancers. *Neuron* 92:1252–1265.
- Risso D, Ngai J, Speed TP, Dudoit S (2014) Normalization of RNA-seq data using factor analysis of control genes or samples. *Nat Biotechnol* 32:896–902.
- Robinson MD, McCarthy DJ, Smyth GK (2010) edgeR: a bioconductor package for differential expression analysis of digital gene expression data. *Bioinformatics* 26:139–140.
- Rosa AI, Gonçalves J, Cortes L, Bernardino L, Malva JO, Agasse F (2010) The angiogenic factor angiopoietin-1 is a proneurogenic peptide on subventricular zone stem/progenitor cells. *J Neurosci* 30:4573–4584.
- Rubenstein JRL, Campbell K (2020) Neurogenesis in the basal ganglia. In: *Patterning and cell type specification in the developing CNS and PNS*, Ed 2 (Rubenstein JRL, Rakic P, Chen B, Kwan K, eds), pp 399–426. London: Academic.
- Sakaue Y, Sanada M, Sasaki T, Kashiwagi A, Yasuda H (2003) Amelioration of retarded neurite outgrowth of dorsal root ganglion neurons by overexpression of PKCdelta in diabetic rats. *Neuroreport* 14:431–436.
- Shinwari JM, Khan A, Awad S, Shinwari Z, Alaiya A, Alanazi M, Tahir A, Poizat C, Al Tassan N (2015) Recessive mutations in *COL25A1* are a cause of congenital cranial dysinnervation disorder. *Am J Hum Genet* 96:147–152.
- Siddiqi F, Trakimas AL, Joseph DJ, Lippincott ML, Marsh ED, Wolfe JH (2021) *Isl1* precursors contribute to mature interneuron subtypes in mouse neocortex. *Cereb Cortex* 31:5206–5224.
- Simpson TI, Pratt T, Mason JO, Price DJ (2009) Normal ventral telencephalic expression of *Pax6* is required for normal development of thalamocortical axons in embryonic mice. *Neural Dev* 4:19.
- Smith-Swintosky VL, Zimmer S, Fenton JW 2nd, Mattson MP (1995) Protease nexin-1 and thrombin modulate neuronal Ca^{2+} homeostasis and sensitivity to glucose deprivation-induced injury. *J Neurosci* 15:5840–5850.
- Snijders Blok L, Vano A, den Hoed J, Underhill HR, Monteil D, Li H, Reynoso Santos FJ, Chung WK, Amaral MD, Schnur RE, Santiago-Sim T, Si Y, Brunner HG, Kleefstra T, Fisher SE (2021) Heterozygous variants that disturb the transcriptional repressor activity of *FOXP4* cause a developmental disorder with speech/language delays and multiple congenital abnormalities. *Genet Med* 23:534–542.
- Spead O, Poulain FE (2020) Trans-axonal signaling in neural circuit wiring. *Int J Mol Sci* 21:5170.
- Stoykova A, Fritsch R, Walther C, Gruss P (1996) Forebrain patterning defects in small eye mutant mice. *Development* 122:3453–3465.
- Tanaka T, Wakabayashi T, Oizumi H, Nishio S, Sato T, Harada A, Fujii D, Matsuo Y, Hashimoto T, Iwatsubo T (2014) *CLAC-P/collagen type XXV* is required for the intramuscular innervation of motoneurons during neuromuscular development. *J Neurosci* 34:1370–1379.
- Taniguchi H, He M, Wu P, Kim S, Paik R, Sugino K, Kvitsiani D, Kvitsani D, Fu Y, Lu J, Lin Y, Miyoshi G, Shima Y, Fishell G, Nelson SB, Huang ZJ (2011) A resource of Cre driver lines for genetic targeting of GABAergic neurons in cerebral cortex. *Neuron* 71:995–1013.
- Thor S, Ericson J, Brännström T, Edlund T (1991) The homeodomain LIM protein *Isl-1* is expressed in subsets of neurons and endocrine cells in the adult rat. *Neuron* 7:881–889.
- Tinterri A, Menardy F, Diana MA, Lokmane L, Keita M, Couplier F, Lemoine S, Mailhes C, Mathieu B, Merchan-Sala P, Campbell K, Gyory I, Grosschedl R, Popa D, Garel S (2018) Active intermixing of indirect and direct neurons builds the striatal mosaic. *Nat Commun* 9:4725.
- Toma JS, Karamboulas K, Carr MJ, Kolaj A, Yuzwa SA, Mahmud N, Storer MA, Kaplan DR, Miller FD (2020) Peripheral nerve single-cell analysis identifies mesenchymal ligands that promote axonal growth. *eNeuro* 7:ENEURO.0066-20.2020.
- Tuttle R, Nakagawa Y, Johnson JE, O'Leary DD (1999) Defects in thalamocortical axon pathfinding correlate with altered cell domains in *Mash-1*-deficient mice. *Development* 126:1903–1916.
- Uemura M, Nakao S, Suzuki ST, Takeichi M, Hirano S (2007) *OL-Protocadherin* is essential for growth of striatal axons and thalamocortical projections. *Nat Neurosci* 10:1151–1159.
- Visel A, Thaller C, Eichele G (2004) GenePaint.org: an atlas of gene expression patterns in the mouse embryo. *Nucleic Acids Res* 32:D552–D556.

- Waclaw RR, Allen ZJ, 2nd, Bell SM, Erdélyi F, Szabó G, Potter SS, Campbell K (2006) The zinc finger transcription factor Sp8 regulates the generation and diversity of olfactory bulb interneurons. *Neuron* 49:503–516.
- Waclaw RR, Ehrman LA, Merchan-Sala P, Kohli V, Nardini D, Campbell K (2017) Foxo1 is a downstream effector of Isl1 in direct pathway striatal projection neuron development within the embryonic mouse telencephalon. *Mol Cell Neurosci* 80:44–51.
- Walsh KB, Zhang X, Zhu X, Wohleb E, Woo D, Lu L, Adeoye O (2019) Intracerebral hemorrhage induces inflammatory gene expression in peripheral blood: global transcriptional profiling in intracerebral hemorrhage patients. *DNA Cell Biol* 38:660–669.
- Walter W, Sánchez-Cabo F, Ricote M (2015) GOpilot: an R package for visually combining expression data with functional analysis. *Bioinformatics* 31:2912–2914.
- Wolman MA, Liu Y, Tawarayama H, Shoji W, Halloran MC (2004) Repulsion and attraction of axons by semaphorin3D are mediated by different neuropilins *in vivo*. *J Neurosci* 24:8428–8435.
- Wolman MA, Regnery AM, Becker T, Becker CG, Halloran MC (2007) Semaphorin3D regulates axon interactions by modulating levels of L1 cell adhesion molecule. *J Neurosci* 27:9653–9663.
- Yun K, Garel S, Fischman S, Rubenstein JL (2003) Patterning of the lateral ganglionic eminence by the Gsh1 and Gsh2 homeobox genes regulates striatal and olfactory bulb histogenesis and the growth of axons through the basal ganglia. *J Comp Neurol* 461:151–165.
- Zhang Z, Wei S, Du H, Su Z, Wen Y, Shang Z, Song X, Xu Z, You Y, Yang Z (2019) Zfhx3 is required for the differentiation of late born D1-type medium spiny neurons. *Exp Neurol* 322:113055.